Philosophical Magazine
Vol. 00, No. 00, 00 Month 200x, 1–37

RESEARCH ARTICLE

On the macroscopic response, microstructure evolution, and macroscopic stability of short-fiber-reinforced elastomers at finite strains: I—Analytical results

Reza Avazmohammadi, Pedro Ponte Castañeda

Department of Mechanical Engineering and Applied Mechanics, University of Pennsylvania, Philadelphia, PA 19104-6315, U.S.A.

(*Received 00 Month 200x; final version received 00 Month 200x*)

This paper presents a homogenization-based constitutive model for the mechanical behavior of particle-reinforced elastomers with random microstructures subjected to finite deformations. The model is based on a recently improved version of the tangent second-order (TSO) method (Avazmohammadi and Ponte Castaneda 2013; J. Elasticity 112, 1828–1850) for two-phase, hyperelastic composites, and is able to directly account for the shape, orientation, and concentration of the particles. After a brief summary of the TSO homogenization method, we describe its application to composites consisting of an incompressible rubber reinforced by aligned, spheroidal, rigid particles, undergoing generally non-aligned, three-dimensional loadings. While the results are valid for finite particle concentrations, in the dilute limit they can be viewed as providing a generalization of Eshelby's results in linear elasticity. In particular, we provide analytical estimates for the overall response and microstructure evolution of the particle-reinforced composites with generalized neo-Hookean matrix phases under non-aligned loadings. For the special case of aligned pure shear and axisymmetric shear loadings, we give closed-form expressions for the effective stored-energy function of the composites with neo-Hookean matrix behavior. Moreover, we investigate the possible development of "macroscopic" (shear band-type) instabilities in the homogenized behavior of the composite at sufficiently large deformations. These instabilities whose wavelengths are much larger than the typical size of the microstructure are detected by making use of the loss of strong ellipticity condition for the effective stored-energy function of the composites. The analytical results presented in this paper will be complemented in Part II of this work by specific applications for several representative microstructures and loading configurations.

Keywords: composite materials; particulate microstructure; homogenization; nonlinear elasticity; shear band instabilities

1. Introduction

Soft, heterogeneous materials that can undergo large deformations constitute an extensively utilized class of materials in engineering applications, as well as a large class of naturally existing material systems. Particle- and fiber-reinforced elastomers are a prominent class of soft materials that have found a wide range of applications in industry. A few examples of such applications include car tires, flexible underwater vehicles, and compliant aircraft structures. In particular, carbon-filled and silica-filled rubbers are two important groups of particle-reinforced elastomers used for technological purposes [6, 17, 30, 42]. Moreover, elastomer-like, heterogeneous materials with particulate/fibrous microstructures are also naturally present in the form of biological tissues, such as arterial walls, ligaments, annulus fibrosus, etc. [see, e.g., 9, 18, 19, 37].

As a consequence, investigations to characterize the mechanical behavior of elastomeric composites are very timely. This work is concerned with establishing relations between the underlying microstructure of these materials and their macroscopic response, by means of homogenization. To date, there are essentially two types of homogenization approaches that can be brought to bear on this problem. The first type is based on

ISSN: 1478-6435 print/ISSN 1478-6443 online

DOI: 10.1080/14786435.20xx.xxxxxx
http://www.informaworld.com

the "linear comparison" variational methods, including the so-called "tangent second-order" (TSO) method [4, 16, 35] and the "generalized second-order" (GSO) technique [23, 24, 32]. These methods make use of suitably designed variational principles for the properties of appropriately defined "linear comparison composites" (LCC), which are fictitious composites with the same microstructure as the original nonlinear composites, but with linear properties. The distinguishing features of the second-order methods are that: (1) they rigorously incorporate full dependence on the nonlinear constitutive behavior of the constituent phases, (2) they are exact to second-order in the heterogeneity contrast (hence their name), and (3) they account for statistical information about the underlying microstructure in the undeformed configuration, as well as for its evolution, resulting from the finite changes in geometry caused by the applied finite deformations. The latter is essential in homogenization of hyperelastic composites as the *evolution of the microstructure* can have significant geometric softening or stiffening effects on the overall response of the material, which, in turn, may lead to the possible development of *macroscopic instabilities*. The second type of approach is based on sequential lamination, which has been used extensively for linear composites to demonstrate optimality of bounds [28], and has been used more recently in the context of finite elasticity [10, 11, 22]. These iterated methods have the distinct advantage of producing "exact" results, unlike the linear comparison methods, which only provide variational approximations. However, the classes of microstructures that can be considered are much more restrictive and there is no precise control on the typical microstructural variables such as particle shape. Instead, use is made of two-point correlation functions for the particulate phase, which typically exhibits highly distorted and physically unrealistic shapes. In addition, this technique generally leads to partial differential equations (of the Hamilton-Jacobi type) for the effective behavior, which have only been solved exactly for some very special geometric configurations and very specific constitutive models (essentially, neo-Hookean). More generally, numerical (or other types of approximations) are required to obtain explicit results by the lamination methods. By contrast, the linear comparison methods can handle much more general classes of constitutive behavior for the phases, as well as microstructures, including, for example, polydomain elastomeric systems [38].

Given the highly nonlinear character of these homogenization problems in finite elasticity, the first applications were carried out in the context of two-dimensional idealizations of the microstructure. Thus, elastomers with random and periodic distributions of circular particles were first considered by Ponte Castañeda and Tiberio [35] and Lahellec et al. [16], respectively. Corresponding estimates for sequentially laminated microstructures were investigated by deBotton [10]. These works showed that the rigid particles have the expected reinforcing effect, although the linear comparison estimates provided a significantly stronger reinforcing effect compared to the sequentially laminated microstructures. In fact, the first type of estimate predicted a certain type of "geometric" locking up of the macroscopic response, which has since been found to be physically unrealistic, while the second type of estimate predicted—somewhat surprisingly—for a neo-Hookean matrix phase the same dependence on the volume fraction, as for the corresponding linear case. For the purposes of the present work, the most relevant work was carried out by Lopez-Pamies and Ponte Castañeda [25] for random distributions of rigid elliptical fibers in an elastomeric phase, or more precisely for plane strain loading of continuous fiber-reinforced elastomers in the transverse plane where the fibers exhibit elliptical cross-section. These estimates, which are free from geometric locking up, demonstrated for the first time the strong effect of particle rotations, which, under certain conditions, could induce strong geometric softening leading to the possible development of macroscopic instabilities through loss of ellipticity. These homogenization estimates were also compared with full-field numerical simulations by Moraleda et al. [29] and found to be in fairly good quantitative agreement at least for neo-Hookean matrix phases.

The existence of long wave length instabilities [14], as well as other types of "microscopic" instabilities, in the context of two-dimensional fiber-reinforced composites with periodic microstructures has also been documented recently [27]. Further applications of these methods for fiber-reinforced composites containing periodic and random distributions of cylindrical fibers (or circular cross section) in an elastomeric matrix subjected to more general three-dimensional loading conditions have been addressed more recently by means of the GSO method [2, 3, 8]. In addition, estimates for the macroscopic behavior of hyperelastic matrices reinforced with aligned cylindrical fibers have also been obtained making use of the sequentially laminated structures, as well as composite-cylinder assemblages [11, 12, 22, 39]. Results for particle-reinforced elastomers with spherical inclusions subjected to general three-dimensional loading conditions have only been generated more recently using the linear comparison homogenization method [4, 7], and using a combination of the sequential lamination and generalized self-consistent method [20, 21].

In spite of the significant progress over the last 12 years, results are not yet available for more general microstructures and indeed this is the central objective of the present work. In particular, we seek to investigate the effect of particle shape on the macroscopic response, microstructure evolution and macroscopic instabilities in short-fiber-reinforced elastomers subjected to general finite-strain loadings. For this purpose, we will make use of the recent work of Avazmohammadi and Ponte Castañeda [4], which provided a more robust way of handling the incompressibility of the elastomeric matrix phase in the context of the tangent second-order procedure that the one initially proposed by Ponte Castañeda and Tiberio [35]. Thus, the resulting estimates for the macroscopic response of the reinforced elastomers are consistent with the overall incompressibility constraint, expected on physical grounds. On the other hand, the new method preserves the advantages of the linear comparison approaches, allowing the direct conversion of classical results for linear elastic composites—including estimates of the Eshelby and Willis type for systems reinforced with ellipsoidal inclusions—into corresponding estimates for the nonlinear, hyperelastic composites. Remarkably, the nonlinear homogenization theory is able to provide analytical estimates for the evolution of the relevant microstructural variables, including most notably the rotation of the ellipsoidal particles under general loading conditions. In particular, it was verified [4] that the improved version of the TSO method leads to predictions that are very similar—and in some cases identical—to the predictions of the more sophisticated GSO method [24], at least for the case of two-dimensional elliptical particles [25]. In this context, it should be noted that the GSO method requires the use of the field fluctuations in the linear comparison composite and is therefore more difficult to implement, especially for the complex three-dimensional microstructures of interest in this work.

The structure of the paper is as follows. For convenience and clarity, Sections 2 and 3 summarize the basic elements of the nonlinear homogenization methods and, in particular, the tangent second-order theory [4]. Section 4 deals with the specific application of the TSO theory for elastomers reinforced with aligned, rigid, spheroidal particles. This section includes closed-form, analytical expressions for the homogenized stored-energy function of transversely isotropic, reinforced elastomers with neo-Hookean matrix phases under aligned, triaxial loading conditions (see expressions (35), (39), and (42)). Section 5 spells out the general conditions of strong ellipticity used to determine the "macroscopic" instabilities for incompressible, transversely isotropic, hyperelastic composites under aligned and non-aligned loading conditions. These conditions are provided in terms of appropriate traces of the associated effective incremental modulus tensor, which, in turn, can be written in terms of the derivatives of the associated effective stored-energy function with respect to the macroscopic kinematical variables. Then, these conditions are specialized for the class of (rigid) particle-reinforced elastomers undergoing *axisymmetric* and *pure* shear loading conditions. Finally, some conclusions are drawn in Section 6. In Part II of

this paper, use will be made of the analytical results presented in Secs. 4 and 5 of this paper to investigate in more detail the influence of the microgeometry, matrix properties, and loading conditions on the effective constitutive behavior of the reinforced elastomers, including the associated microstructure evolution and the possible development of macroscopic instabilities.

2. Preliminaries on hyperelastic composites and their effective behavior

Consider a specimen consisting of several families of aligned, ellipsoidal particles, distributed randomly in a matrix phase, and occupying a volume Ω_0 with boundary $\partial\Omega_0$ in the undeformed configuration. Following the hypothesis of *separation of length scales*, we will assume that the characteristic length-scale of the particles is much smaller than the size of the specimen as well as the scale of variation of the loading conditions. Let the position vector of a material point in the undeformed configuration Ω_0 be denoted by $\mathbf{X}$, with Cartesian components X_i, $i \in \{1,2,3\}$, and the corresponding position vector in the deformed configuration Ω be denoted by $\mathbf{x}$, with components x_i. The deformation gradient tensor represented by $\mathbf{F}$ has components $F_{ij} = \partial x_i/\partial X_j$ and is required to satisfy the material *impenetrability* condition: $J = \det\mathbf{F}(\mathbf{X}) > 0$ for all $\mathbf{X} \in \Omega_0$. In addition, let $\mathbf{F} = \mathbf{R}\,\mathbf{U}$ where $\mathbf{U}$ and $\mathbf{R}$ stand for the stretch and (*rigid-body*) rotation tensors, respectively, and let $\mathbf{C} = \mathbf{F}^T\mathbf{F} = \mathbf{U}^2$ denote the right Cauchy–Green deformation tensor.

We assume that the constitutive behavior of the phases is purely elastic and characterized by the stored-energy functions $W^{(r)}(\mathbf{F})\,(r = 1,...,N)$, which are taken to be *non-convex* functions of the deformation gradient tensor $\mathbf{F}$. Also, the stored-energy functions $W^{(r)}(\mathbf{F})$ are assumed to be objective, namely, $W^{(r)}(\mathbf{Q}\mathbf{F}) = W^{(r)}(\mathbf{F})$ for all proper orthogonal tensors $\mathbf{Q}$ and arbitrary deformation gradients $\mathbf{F}$, so that $W^{(r)}(\mathbf{F}) = W^{(r)}(\mathbf{U})$. In this work, we restrict our attention to the special case of composites made up of incompressible isotropic phases, and it proves useful, for later use, to introduce the following decomposition for the stored-energy function

$$W^{(r)}(\mathbf{F}) = W_\mu^{(r)}(\mathbf{F}) + \frac{1}{2}\mu'^{(r)}(J-1)^2, \tag{1}$$

where $W_\mu^{(r)}$ denotes the "distortional" component of $W^{(r)}$ and depends on the ground-state shear modulus $\mu^{(r)}$, while the second term depending on the Lamé parameter $\mu'^{(r)}$ characterizes the "volumetric" response of phase r. In other words, $W_\mu^{(r)}$ is that part of the stored-energy function $W^{(r)}$ which does not depend on $\mu'^{(r)}$. It is a simple matter to verify from (1) that the incompressibility constraint $J = 1$ is recovered by letting the parameter $\mu'^{(r)}$ tend to infinity.

The first Piola-Kirchhoff stress in phase r is then given by the expression

$$\mathbf{S} = \frac{\partial W^{(r)}}{\partial \mathbf{F}}(\mathbf{F}). \tag{2}$$

In this connection, it is useful to also define

$$\mathbf{S}_\mu^{(r)}(\mathbf{F}) = \frac{\partial W_\mu^{(r)}}{\partial \mathbf{F}}(\mathbf{F}), \tag{3}$$

such that

$$\mathbf{S} = \mathbf{S}_\mu^{(r)}(\mathbf{F}) + \mu'^{(r)}J(J-1)\mathbf{F}^{-T}. \tag{4}$$

In addition, consistent with the definition (1), the incremental *tangent* modulus tensor for the phase r can be decomposed as

$$\mathbf{L}^{(r)}(\mathbf{F}) = \frac{\partial^2 W^{(r)}}{\partial \mathbf{F}\,\partial \mathbf{F}} = \mathbf{L}_{\mu}^{(r)} + \mu'^{(r)}\mathbf{L}_{-1}^{(r)}, \tag{5}$$

where

$$\mathbf{L}_{\mu}^{(r)}(\mathbf{F}) = \frac{\partial^2 W_{\mu}^{(r)}}{\partial \mathbf{F}\,\partial \mathbf{F}}, \quad \text{and} \quad \mathbf{L}_{-1}^{(r)}(\mathbf{F}) = J(2J-1)\mathbf{F}^{-T}\otimes\mathbf{F}^{-T} + J(J-1)\mathscr{X}, \tag{6}$$

with $\mathscr{X}$ denoting the fourth-order tensor with components $\mathscr{X}_{ijkl} = -F_{li}^{-1}F_{jk}^{-1}$.

Next, the local energy function of the composite is defined as

$$W(\mathbf{X},\mathbf{F}) = \sum_{r=1}^{N} \chi^{(r)}(\mathbf{X})\, W^{(r)}(\mathbf{F}), \tag{7}$$

where the characteristic functions $\chi^{(r)}$, describing the distribution of the phases in the reference configuration, are such that they equal 1 if the position vector $\mathbf{X}$ is inside the phase r (*i.e.*, $\mathbf{X}\in\Omega_0^{(r)}$) and zero otherwise. Following [15], the effective, or macroscopic stored-energy function $\widetilde{W}$ of the composite elastomer is given by

$$\widetilde{W}(\bar{\mathbf{F}}) = \min_{\mathbf{F}\in K(\bar{\mathbf{F}})} \langle W(\mathbf{X},\mathbf{F})\rangle = \min_{\mathbf{F}\in K(\bar{\mathbf{F}})} \sum_{r=1}^{N} c_0^{(r)} \left\langle W^{(r)}(\mathbf{F})\right\rangle^{(r)}, \tag{8}$$

where $K(\bar{\mathbf{F}})$ denotes the set of kinematically admissible deformation gradients defined by

$$K(\bar{\mathbf{F}}) = \left\{\mathbf{F}\,|\,\exists \mathbf{x}=\mathbf{x}(\mathbf{X}) \text{ with } \mathbf{F}=\operatorname{Grad}\mathbf{x} \text{ and } J>0 \text{ in } \Omega_0,\ \mathbf{x}=\bar{\mathbf{F}}\mathbf{X} \text{ on } \partial\Omega_0\right\}. \tag{9}$$

In the above expressions, the triangular brackets $\langle\cdot\rangle$ represent volume averages (in the undeformed configuration) over a representative volume element (RVE) Ω_0 of the composite, while $\langle\cdot\rangle^{(r)}$ denote volume averages (in the undeformed configuration) over the phases $\Omega_0^{(r)}$, so that the scalar $c_0^{(r)} = \left\langle \chi^{(r)}\right\rangle$ indicates the initial volume fraction of the phase r. Noting that under the above-defined affine boundary condition $\langle\mathbf{F}\rangle = \bar{\mathbf{F}}$, and defining the average stress $\bar{\mathbf{S}} = \langle\mathbf{S}\rangle$, the effective constitutive relation for the composite is then given by [15]

$$\bar{\mathbf{S}} = \frac{\partial \widetilde{W}}{\partial \bar{\mathbf{F}}}(\bar{\mathbf{F}}). \tag{10}$$

At this point, it should be remarked that the solution (assuming that it exists) of the Euler-Lagrange equations associated with the variational problem (8) is expected to be unique in some neighborhood of $\bar{\mathbf{F}}=\mathbf{I}$ (where $\mathbf{I}$ is the second-order identity tensor), and gives the minimum energy. However, as the deformation increases into the finite deformation regime, it may reach a point at which the solution of the Euler-Lagrange equations (referred to as the "principal" solution and denoted by $\widehat{W}(\bar{\mathbf{F}})$) is not unique anymore, and other kinematically admissible solutions corresponding to a lower energy might exist (which, according to (8), is labeled $\widetilde{W}$). This point corresponds to the possible onset of an *instability*, beyond which the applicability of the "principal" solution becomes questionable. In the context of hyperelastic composites with periodic microstructures, it is known [14, 41] that the first instability may be "microscopic" with wavelengths comparable to the

size of the inhomogeneities, or they may be "macroscopic" with wavelengths comparable to the size of the RVE. However, for composites with random microstructures, it may be expected [27] that the first instability should actually be macroscopic. On the other hand, it is also known [14, 40] that the "macroscopic" instabilities can be determined from the loss of *strong ellipticity* of the effective stored-energy function of the material evaluated at the above-described "principal" solution. For these reasons, in this work we will only be concerned with the principal solution $\widehat{W}$, whose range of validity will be estimated by evaluation of the associated loss of ellipticity condition.

Following up on the preceding remarks, we finish this section by spelling out the condition of strong ellipticity (SE) for the effective stored-energy function $\widehat{W}(\bar{\mathbf{F}})$. In the context of hyperelastic materials, the SE condition for the homogenized composite elastomers characterized by the stored-energy function $\widehat{W}(\bar{\mathbf{F}})$ is equivalent to the positive-definiteness of the associated acoustic tensor $\widehat{\mathbf{K}}$, namely, $\widehat{W}(\bar{\mathbf{F}})$ is said to be *strongly elliptic* if and only if

$$\widehat{K}_{ik}\, m_i m_k = \widehat{L}_{ijkl}\, N_j N_l\, m_i m_k > 0, \tag{11}$$

for all non-zero pairs of unit vectors $\mathbf{N}$ and $\mathbf{m}$. Here, $\widehat{K}_{ik} = \widehat{L}_{ijkl}\, N_j N_l$ is the effective acoustic tensor, and, the fourth-order tensor $\widehat{\mathbf{L}}$, defined by

$$\widehat{\mathbf{L}} = \frac{\partial^2 \widehat{W}}{\partial \bar{\mathbf{F}}\, \partial \bar{\mathbf{F}}}, \tag{12}$$

denotes the incremental effective moduli tensor of the composite material characterizing the overall incremental response of the composite elastomer. It is also worth mentioning that the tensor $\widehat{L}_{ijkl}$ possesses major symmetry ($\widehat{L}_{ijkl} = \widehat{L}_{klij}$), but not generally minor symmetries ($\widehat{L}_{ijkl} \neq \widehat{L}_{jilk}$).

3. Tangent second-order homogenization estimates

In this section, we briefly recall the recently developed tangent second-order variational method of Avazmohammadi and Ponte Castañeda [4] for the effective constitutive behavior of (two-phase) particle-reinforced, hyperelastic composites consisting of aligned, ellipsoidal, rigid particles distributed randomly with volume fraction c in an incompressible matrix phase with energy function $W_\mu^{(1)}$. (Note that since particles are rigid and the matrix is incompressible, $c = c_0^{(2)}$ for all macroscopic deformations.) As already mentioned, the TSO method makes use of a fictitious "linear comparison composite" (LCC) with the same microstructure (i.e., same characteristic functions $\chi^{(r)}(\mathbf{X})$) as the actual (nonlinear) composite material (in the undeformed configuration). The moduli of the constituent phases in the LCC are identified with "tangent" linearizations of the given nonlinear phases evaluated at the macroscopic deformation gradient $\bar{\mathbf{F}}$. This allows the use of already available methods for estimating the effective behavior of linear composites to generate corresponding estimates for nonlinear composites. Avazmohammadi and Ponte Castañeda [4] made use of the generalized Hashin-Shtrikman estimates of the Willis type [36, 43] for the effective behavior of the linear-elastic composite materials consisting of random distributions of aligned ellipsoidal particles with prescribed "ellipsoidal symmetry" for the particle centers (i.e., the two-point correlation functions). These estimates are exact to second-order in the heterogeneity contrast and to first order in the particle volume fraction, and are known to be quite accurate for the type of "particulate" microstructures of interest here, up to moderate concentrations of particles. In order to ensure compliance with the overall incompressibility constraint ($\bar{J} = \det(\bar{\mathbf{F}}) = 1$), Avazmohammadi and

Ponte Castañeda [4] made use of the expression (1) to split the distortional and deviatoric components of the energy and arrived at the following estimate for the effective stored-energy function $\widehat{W}(\bar{\mathbf{F}})$ of the reinforced elastomers:

$$\widehat{W}(\bar{\mathbf{F}}) = (1-c)W_{\mu}^{(1)}(\bar{\mathbf{F}}^{(1)}) + \frac{1}{2}\frac{c}{1-c}(\bar{\mathbf{F}} - \bar{\mathbf{R}}^{(2)}) \cdot \mathbf{E}\,(\bar{\mathbf{F}} - \bar{\mathbf{R}}^{(2)}). \tag{13}$$

In this expression, $\bar{\mathbf{F}}$ is the macroscopic deformation which satisfies the incompressibility condition $\det(\bar{\mathbf{F}}) = 1$, $\bar{\mathbf{R}}^{(2)}$ is a second-order orthogonal tensor characterizing the average rotation of the rigid particles under the macroscopic deformation gradient $\bar{\mathbf{F}}$, and determined by the kinematical equation

$$Skew\left\{(\bar{\mathbf{R}}^{(2)})^T[\mathbf{E}\,(\bar{\mathbf{F}} - \bar{\mathbf{R}}^{(2)})] + (1-c)(\bar{\mathbf{R}}^{(2)})^T\,\mathbf{S}_{\mu}^{(1)}(\bar{\mathbf{F}}^{(1)})\right\} = \mathbf{0}, \tag{14}$$

where *Skew* denotes the skew-symmetric part of the quantities inside the curly brackets. Note that equation (14) provides in general a set of three scalar algebraic equations for the three independent components of $\bar{\mathbf{R}}^{(2)}$. The second-order tensor $\bar{\mathbf{F}}^{(1)}$ corresponds to the average deformation gradient in the matrix phase of the LCC, which can be expressed in terms of the macroscopic deformation gradient $\bar{\mathbf{F}}$, and the rotation tensor $\bar{\mathbf{R}}^{(2)}$ as

$$\bar{\mathbf{F}}^{(1)} = \frac{1}{1-c}(\bar{\mathbf{F}} - c\,\bar{\mathbf{R}}^{(2)}), \tag{15}$$

Finally, $\mathbf{E}$ is a fourth-order, microstructural tensor given by[1]

$$\mathbf{E} = \lim_{\mu'^{(1)} \to \infty} (\mathbf{P}^{-1} - \mathbf{L}^{(1)}). \tag{16}$$

In this relation, $\mathbf{L}^{(1)}$ is a fourth-order moduli tensor determined by the tangent modulus evaluated at the macroscopic deformation, such that

$$\mathbf{L}^{(1)} = \frac{\partial^2 W^{(1)}}{\partial \mathbf{F}\,\partial \mathbf{F}}(\bar{\mathbf{F}}), \tag{17}$$

while $\mathbf{P}$ is an Eshelby-type (fourth-order) tensor containing information about the shape and distribution of the particles in the undeformed configuration [36]. For ellipsoidal particles, distributed in an infinite matrix with the elastic modulus tensor $\mathbf{L}^{(1)}$, the components of $\mathbf{P}$ read as

$$P_{ijkl} = \frac{1}{4\pi\,|\mathbf{Z}_0|}\int_{|\boldsymbol{\xi}|=1} B_{ik}(\boldsymbol{\xi})\,\xi_j\xi_l\left[\boldsymbol{\xi}^T(\mathbf{Z}_0^T\,\mathbf{Z}_0)^{-1}\boldsymbol{\xi}\right]^{\frac{-3}{2}} dS, \tag{18}$$

where the symmetric, second-order tensor $\mathbf{Z}_0$ serves to characterize the "shape" and "orientation" of the particles in the undeformed configuration, and the tensor $\mathbf{B}$ denotes the inverse of the acoustic tensor $\mathbf{K}$ of the matrix with components $K_{ik} = L_{ijkl}^{(1)}\,\xi_j\xi_l$. In this work, we will also assume that the initial (in the undeformed configuration) "shape" and "orientation" of the two-point correlation function for the distribution of the ellipsoidal particles are identically the same as for the particles themselves, as specified by the tensor $\mathbf{Z}_0$. It should be remarked that this assumption is not essential, and the shapes and orientations of the distribution functions could, in general, be different from those of the

[1] In the prior work [4], the fourth-order tensor $\mathbf{E}$ was labelled $\mathbf{E}^I$, but, for simplicity, the superscript I has been dropped here.

particles [36] leading to the use of two different $\mathbf{P}$ tensors. It is also worth mentioning that all fourth-order tensors $\mathbf{E}$, $\mathbf{P}$, and $\mathbf{L}^{(1)}$ have major symmetry, but not generally minor symmetry. Furthermore, in view of definitions (16)-(18), together with the objectivity assumption for $W^{(1)}(\mathbf{F})$, it can be verified that

$$E_{ijkl}(\bar{\mathbf{F}}) = \bar{R}_{ip}\bar{R}_{kq}E_{pjql}(\bar{\mathbf{U}}), \tag{19}$$

where $\bar{\mathbf{U}}$ and $\bar{\mathbf{R}}$ denote the macroscopic stretch and (rigid-body) rotation tensors, respectively (note that $\bar{\mathbf{F}} = \bar{\mathbf{R}}\bar{\mathbf{U}}$). Making use of (19) along with (14) and (15), it can be shown that expression (13) for $\widehat{W}(\bar{\mathbf{F}})$ satisfies the *objectivity* condition

$$\widehat{W}(\bar{\mathbf{F}}) = \widehat{W}(\bar{\mathbf{U}}). \tag{20}$$

In summary, for a given ellipsoidal microstructure, macroscopic loading $\bar{\mathbf{F}}$, and matrix strain energy $W^{(1)}$, the computation of the effective stored-energy function $\widehat{W}(\bar{\mathbf{F}})$ in (13), as well as of the associated rotation tensor $\bar{\mathbf{R}}^{(2)}$ in (14), requires the calculation of $\mathbf{E}$. As defined in (16), the tensor $\mathbf{E}$ should be calculated in the incompressibility limit of the matrix phase ($\mu'^{(1)} \to \infty$). To this end, Avazmohammadi and Ponte Castañeda [4] carried out a general asymptotic analysis for the computation of the tensor $\mathbf{E}$ in the incompressibility limit ($\mu'^{(1)} \to \infty$). For completeness and to maintain continuity, the procedure for computing the tensor $\mathbf{E}$ is provided in Appendix A.

We conclude this section by noting that Avazmohammadi and Ponte Castañeda [4] already considered the application of the above-described results for the special case of elastomers reinforced with spherical particles under triaxial loadings, and for the special case of composites with a neo-Hookean matrix, they derived closed-form expressions for the corresponding effective stored-energy function. In addition, they considered elastomers reinforced with two-dimensional fibers of elliptical cross-section under plane-strain loading. For the special case of composites with a neo-Hookean matrix and dilute concentration of fibers, they recovered exactly the results obtained by Lopez-Pamies and Ponte Castañeda [25] using the more sophisticated GSO method. In addition, for finite concentrations of particles and Gent-type matrices, the agreement of the TSO and GSO results was quite good. In the present work, we will consider for the first time applications for elastomers reinforced with three-dimensional spheroidal fibers.

4. Application to composites with rigid spheroidal particles

In the previous section, we summarized the results for estimating the effective stored-energy function and the associated evolution of the microstructure for rigidly reinforced elastomeric composites with general "ellipsoidal microstructure." The aim of this section is to make use of these results to generate corresponding estimates of the Willis-type for elastomers reinforced with a random distribution of aligned, *spheroidal* particles subjected to finite deformations. Our goal here is to provide explicit analytical estimates when possible; otherwise, numerical calculation of the aforementioned estimates is carried out. In the following paragraphs, we provide detailed description on the microstructural configurations, constitutive behavior of the elastomeric matrix phase, and the applied macroscopic loading for the class of composites of interest in this work.

Microstructures. The microstructures to be studied in this work are shown schematically in Fig. 1, and are depicted in the undeformed configuration relative to the Cartesian basis $\{\mathbf{e}_i\}$ describing a fixed laboratory frame. These microstructures consists of aligned

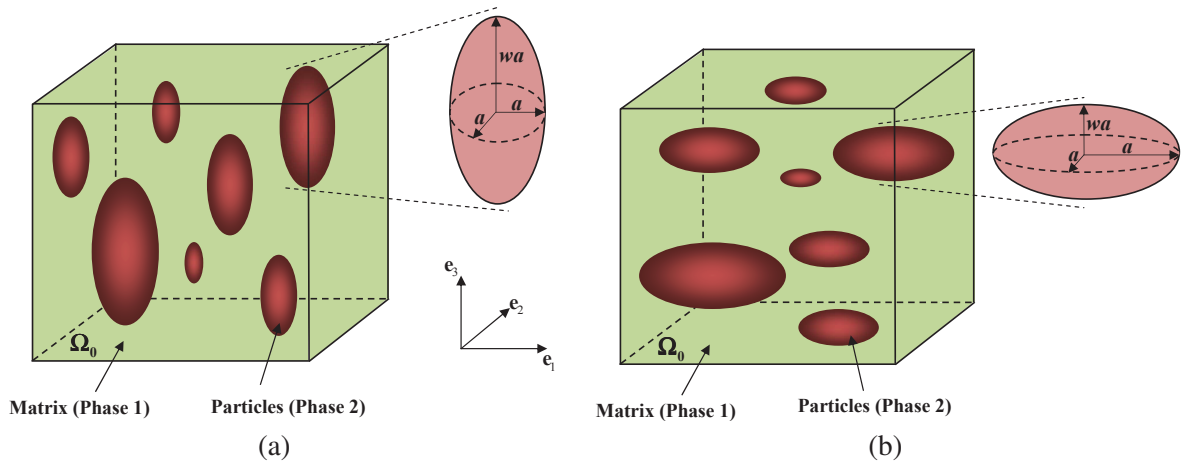

Figure 1. Schematic illustration of the microstructure of a rigid particle-reinforced elastomer in the undeformed configuration (Ω_0). Two configurations are considered. (a) Elastomers reinforced with prolate spheroidal particles ($w > 1$). (b) Elastomers reinforced with oblate spheroidal particles ($w < 1$). Note that, in both cases, the symmetry axis of the particles is initially aligned with the coordinate basis vector $\mathbf{e}_3$.

spheroidal particles of prolate and oblate shapes, in initial volume fraction $c_0^{(2)}$, which remains the same in the deformed configuration ($c = c_0^{(2)}$). As illustrated in Fig. 1(a), the prolate spheroidal particles have aspect ratios $w > 1$, and their major (symmetry) axes are aligned with the $\mathbf{e}_3$-direction. Similarly, as shown in Fig. 1(b), the oblate spheroidal particles have aspect ratios $w < 1$, and their minor (symmetry) axes are likewise aligned with the $\mathbf{e}_3$-direction. Therefore, for both cases, the circular cross-section of the particles in the undeformed configuration lies on the $\mathbf{e}_1 - \mathbf{e}_2$ plane. Moreover, consistent with earlier discussions, it is assumed that the particles are initially distributed with spheroidal symmetry (isotropic symmetry in the transverse plane), and the two-point correlation function of the particle distribution has the same aspect ratio and orientation of those of the particles.

Matrix Constitutive Behavior. The variational estimates (13) and (14) are valid for general behavior for the *incompressible* matrix phase. In this work, for definiteness, attention is restricted to stored-energy functions of the generalized neo-Hookean type, given by expression (1) with

$$W_\mu^{(1)}(\mathbf{F}) = g(I) + h(J). \tag{21}$$

In this expression, $I = \mathrm{tr}(\mathbf{C})$ and, for proper linearization, the material functions $g(I)$ and $h(J)$ are assumed to be twice continuously differentiable satisfying the conditions: $g(3) = h(1) = 0$, $g_I(3) = \mu^{(1)}/2$, $h_J(1) = -\mu^{(1)}$, and $4g_{II}(3) + h_{JJ}(1) = \mu^{(1)}$, in which the subscripts I and J stand for partial differentiation with respect to the invariants I and J, respectively. In particular, we will consider the Gent model [13], which has been shown to provide good agreement with experimental data for rubber-like materials [31] and captures the limiting chain extensibility of elastomers. It is defined by

$$W_\mu^{(1)}(\mathbf{F}) = -\frac{J_m \mu^{(1)}}{2} \ln\left(1 - \frac{I-3}{J_m}\right) + \frac{1}{2}\mu^{(1)}(J-1)(J-3) - \frac{\mu^{(1)}}{J_m}(J-1)^2, \tag{22}$$

where $\mu^{(1)}$ is the ground-state shear modulus and J_m is a the dimensionless parameter characterizing the limiting value for $I-3$ at which the elastomer locks up (and the argument of the logarithm vanishes). In connection with expression (22) for $W_\mu^{(1)}$, it should be emphasized that the terms depending on J, although vanishing for incompressible behav-

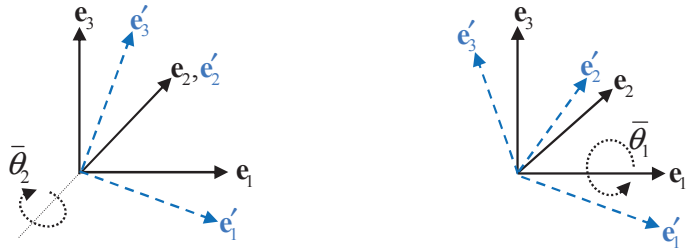

Figure 2. Schematic orientation of the Rectangular coordinate basis $\mathbf{e}'_i$ with respect to the basis $\mathbf{e}_i$ after a two-step rotation. The loading (stretching) directions are aligned with the $\mathbf{e}'_i$ basis vectors, which have a misorientation (measured by angles $\bar{\theta}_1$ and $\bar{\theta}_2$) relative to the $\mathbf{e}_i$ basis.

ior at $J = 1$, are necessary for proper linearization of the deviatoric constitutive response. In addition, we should note that the form (22) used in this work is slightly different from the more common form involving a logarithmic term in J, and indeed used in our prior work [4]. The reason, as we will see below, is that this form leads to better behaved estimates for large values of the deformation. Finally, we note that the Gent model includes the well-known neo-Hookean model in the limit as J_m approaches infinity, where $W_\mu^{(1)}$ specializes to

$$W_\mu^{(1)}(\mathbf{F}) = \frac{1}{2}\mu^{(1)}(I-3) + \frac{1}{2}\mu^{(1)}(J-1)(J-3). \tag{23}$$

Macroscopic Loading. The isotropic distribution of the spheroidal particles in the transverse plane (here, $\mathbf{e}_1 - \mathbf{e}_2$ plane) in the undeformed configuration leads to overall *transversely isotropic* behavior for the composite with symmetry axis $\mathbf{n} = \mathbf{e}_3$. For compressible materials with transversely isotropic symmetry, the strain energy-density function can be written in terms of the 5 proper invariants of the tensor $\bar{\mathbf{C}} = \bar{\mathbf{F}}^T\bar{\mathbf{F}}$ and the vector $\mathbf{n}$ (which reduce to 4 in the incompressibility limit). In this work, we find useful the following decomposition of the macroscopic deformation gradient

$$\bar{\mathbf{F}} = \overline{\mathbf{U}} = \bar{\mathbf{Q}}\,\bar{\mathbf{D}}\,\bar{\mathbf{Q}}^T, \tag{24}$$

where it has been assumed that $\bar{\mathbf{R}} = \mathbf{I}$ with recourse to the overall objectivity (20). In this decomposition, $\bar{\mathbf{D}}$ is a symmetric, second-order tensor given by

$$\bar{\mathbf{D}} = \bar{\lambda}_1\,\mathbf{e}_1 \otimes \mathbf{e}_1 + \bar{\lambda}_2\,\mathbf{e}_2 \otimes \mathbf{e}_2 + \bar{\lambda}_3\,\mathbf{e}_3 \otimes \mathbf{e}_3, \tag{25}$$

with $\bar{\lambda}_1, \bar{\lambda}_2$ and $\bar{\lambda}_3$ identifying the principal values of $\overline{\mathbf{U}}$ (also known as the macroscopic principal stretches). In addition, $\bar{\mathbf{Q}}$ is a proper orthogonal, second-order tensor describing the orientation of the principal axes of $\overline{\mathbf{U}}$ relative to the (fixed) laboratory frame of reference $\{\mathbf{e}_i\}$. Here, the principal axes of the symmetric tensor $\overline{\mathbf{U}}$, also known as the loading (stretching) directions, are identified with the (rectangular Cartesian) basis $\{\mathbf{e}'_i\}$. In general, this basis is not aligned with the basis $\{\mathbf{e}_i\}$, representing the symmetry directions of the particles in the undeformed configuration. In turn, the tensor $\bar{\mathbf{Q}}$ can be decomposed into three proper orthogonal tensor $\bar{\mathbf{Q}}_1, \bar{\mathbf{Q}}_2$, and $\bar{\mathbf{Q}}_3$ serving to characterize the rotations of the principal axes of $\overline{\mathbf{U}}$ about the *fixed* $\mathbf{e}_1$, $\mathbf{e}_2$ and $\mathbf{e}_3$ axis, respectively. Recalling that the composite has transversely isotropic symmetry with symmetry axis along $\mathbf{e}_3$, the response of the composite is insensitive to rotations about $\mathbf{e}_3$, and we can restrict our attention to

tensors $\bar{\mathbf{Q}}$ of the form

$$\bar{\mathbf{Q}} = \bar{\mathbf{Q}}_1\,\bar{\mathbf{Q}}_2. \tag{26}$$

It is important to emphasize that, for a general choice of $\bar{\lambda}_1, \bar{\lambda}_2$ and $\bar{\lambda}_3$, the order of the rotations in (26) matters, and in this work, the order given in (26) will be used. Also, as illustrated in Figure 2, we let the two (Euler) angles $\bar{\theta}_1$ and $\bar{\theta}_2$ denote respectively rotations of the principal axes of $\overline{\mathbf{U}}$ about the $\mathbf{e}_1$ and $\mathbf{e}_2$ axis, with the sign defined according to the usual right-hand rule. More explicitly,

$$\begin{aligned}
\bar{\mathbf{Q}}_1 &= \cos(\bar{\theta}_1)\,(\mathbf{e}_2\otimes\mathbf{e}_2 + \mathbf{e}_3\otimes\mathbf{e}_3) + \sin(\bar{\theta}_1)\,(\mathbf{e}_3\otimes\mathbf{e}_2 - \mathbf{e}_2\otimes\mathbf{e}_3) + \mathbf{e}_1\otimes\mathbf{e}_1,\\
\bar{\mathbf{Q}}_2 &= \cos(\bar{\theta}_2)\,(\mathbf{e}_1\otimes\mathbf{e}_1 + \mathbf{e}_3\otimes\mathbf{e}_3) + \sin(\bar{\theta}_2)\,(\mathbf{e}_1\otimes\mathbf{e}_3 - \mathbf{e}_3\otimes\mathbf{e}_1) + \mathbf{e}_2\otimes\mathbf{e}_2.
\end{aligned} \tag{27}$$

Finally, as mentioned earlier, attention is restricted here to incompressible composite materials satisfying the overall incompressibility constraint, so that

$$\bar{\lambda}_3 = \left(\bar{\lambda}_1\bar{\lambda}_2\right)^{-1}. \tag{28}$$

In terms of the above-defined loading parameters, the effective stored-energy function $\widehat{W}$ may be written in the form

$$\widehat{W}(\bar{\mathbf{F}}) = \widehat{\Phi}(\bar{\lambda}_1, \bar{\lambda}_2, \bar{\theta}_1, \bar{\theta}_2). \tag{29}$$

Moreover, for simplicity, in this work we confine our attention to a subclass of loadings, characterized by the condition $\bar{\theta}_1 = 0^\circ$, as schematically shown in Figure 3. In this case, the effective stored-energy function simplifies further and takes the form

$$\widehat{\phi}(\bar{\lambda}_1, \bar{\lambda}_2, \bar{\theta}) = \widehat{\Phi}(\bar{\lambda}_1, \bar{\lambda}_2, 0, \bar{\theta}), \tag{30}$$

where the parameter $\bar{\theta}_2$ has been replaced by $\bar{\theta}$ for convenience. In this context, it is important to remark that, in general, second and higher derivatives of the effective stored-energy function $\widehat{\Phi}(\bar{\lambda}_1, \bar{\lambda}_2, \bar{\theta}_1, \bar{\theta}_2)$ with respect to $\bar{\theta}_1$, calculated at $\bar{\theta}_1 = 0^\circ$, are required for the calculation of the effective incremental modulus tensor $\widehat{\mathbf{L}}$ (defined in (12)) needed in turn for the computation of the ellipticity condition (11) , even for loadings where $\bar{\theta}_1 = 0^\circ$. For this reason, it will be necessary to compute $\widehat{\Phi}$ for general values of $\bar{\theta}_1$ and $\bar{\theta}_2$, even when the results presented in this work will be restricted to loading paths with $\bar{\theta}_1 = 0^\circ$.

We conclude the description of the macroscopic loading conditions by identifying two special loading conditions: (1) *Axisymmetric Shear*, characterized by the condition $\bar{\lambda}_1 = \bar{\lambda}_2 = \bar{\lambda}$, and (2) *Pure Shear*, characterized by the condition $\bar{\lambda}_2 = 1, \bar{\lambda}_1 = \bar{\lambda}$, where $\bar{\lambda}$ is a positive loading parameter.

4.1. *Estimates for non-aligned loadings*

Under the above-mentioned assumptions on the microstructure, matrix properties and the macroscopic loading, we can now determine the tangent second-order estimates (13) and (14) for the composites consisting of a generalized neo-Hookean matrix (with stored-energy function (21)) and aligned, rigid spheroidal particles, subjected to the applied deformation (24). The resulting estimates, for general stretches $\bar{\lambda}_1$ and $\bar{\lambda}_2$ and angles $\bar{\theta}_1$, and $\bar{\theta}_2$, are too lengthy to be included here, and instead, we present results only for the case of $\bar{\theta}_1 = 0^\circ$ and $\bar{\theta}_2 = \bar{\theta}$. In this case, it can be shown that the estimate for the effective

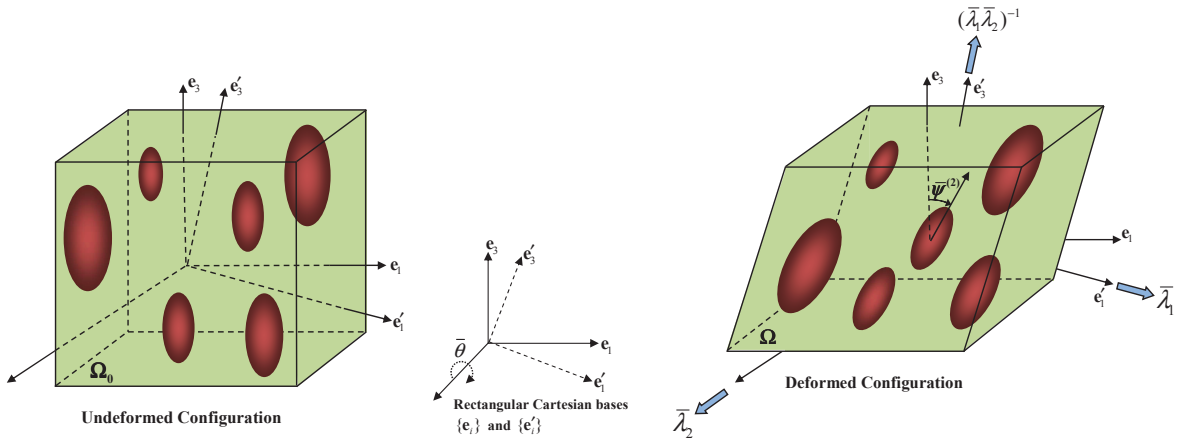

Figure 3. Schematic representation of the applied loading on a rigid particle-reinforced elastomer as well as the associated evolution of microstructure. The loading (stretching) directions are aligned with $\mathbf{e}'_i$ basis vectors which correspond to a rotation $\bar{\theta}$ about the $\mathbf{e}_2$ direction. (a) In the undeformed configuration (Ω_0), the particles are aligned with the $\mathbf{e}_3$ direction. (b) In the deformed configuration (Ω), the particles rotate (by the angle $\bar{\psi}^{(2)}$) on the $\mathbf{e}_1 - \mathbf{e}_3$ plane.

stored-energy function of the composites reduces to

$$\widehat{W}(\bar{\mathbf{F}}) = \widehat{\Phi}(\bar{\lambda}_1,\bar{\lambda}_2,0,\bar{\theta}) = \widehat{\phi}(\bar{\lambda}_1,\bar{\lambda}_2,\bar{\theta}) = (1-c)W_\mu^{(1)}(\bar{\mathbf{F}}^{(1)}) + \frac{c}{2(1-c)}\left\{E_{11}^{11}X_1^2 + (\bar{\lambda}_2-1)^2E_{22}^{22}\right.$$
$$+E_{33}^{33}X_2^2 + E_{13}^{13}Y_1^2 + E_{31}^{31}Y_2^2 + 2\left[X_1(E_{33}^{11}X_2 + E_{13}^{11}Y_1 + E_{31}^{11}Y_2) + X_2(E_{13}^{33}Y_1 + E_{31}^{33}Y_2)\right.$$
$$\left.\left.+(\bar{\lambda}_2-1)\left(E_{22}^{11}X_1 + E_{33}^{22}X_2 + E_{13}^{22}Y_1 + E_{31}^{22}Y_2\right) + E_{31}^{13}Y_1Y_2\right]\right\}, \tag{31}$$

where use has been made of the notation $E_{kl}^{ij} = E_{ijkl}$ for compactness of the Cartesian components of the microstructural tensor $\mathbf{E}$, as defined by expression (16), and where

$$X_1 = \bar{\lambda}_1\cos^2(\bar{\theta}) + \left(\bar{\lambda}_1\bar{\lambda}_2\right)^{-1}\sin^2(\bar{\theta}) - \cos(\bar{\psi}^{(2)}),$$
$$X_2 = \bar{\lambda}_1\sin^2(\bar{\theta}) + \left(\bar{\lambda}_1\bar{\lambda}_2\right)^{-1}\cos^2(\bar{\theta}) - \cos(\bar{\psi}^{(2)}),$$
$$Y_{1,2} = \sin(\bar{\theta})\cos(\bar{\theta})\left[\bar{\lambda}_1 - \left(\bar{\lambda}_1\bar{\lambda}_2\right)^{-1}\right] \pm \sin(\bar{\psi}^{(2)}). \tag{32}$$

In this expressions, $\bar{\psi}^{(2)}$ characterizes the average rotation of the symmetry axis of the particles about the (fixed) $\mathbf{e}_2$ axis (with sign determined by the right-hand rule) in the deformed configuration (see Fig. 3(b)). According to expression (14), $\bar{\psi}^{(2)}$ is determined as the solution of the equation

$$\left[2e_{31}\sin(\bar{\psi}^{(2)}) - f_1X_1 - f_3X_2 + E_{31}^{31}Y_2 - E_{13}^{13}Y_1 - (\bar{\lambda}_2-1)f_2\right]\cos(\bar{\psi}^{(2)})$$
$$-\left\{\left(E_{13}^{11} + E_{13}^{33} + e_{13}\right)Y_1 + E_{11}^{11}X_1 + E_{33}^{33}X_2 + (\bar{\lambda}_2-1)\left(E_{33}^{22} + E_{22}^{11}\right)\right.$$
$$\left.+\left[\bar{\lambda}_1 + \left(\bar{\lambda}_1\bar{\lambda}_2\right)^{-1}\right]\left[E_{33}^{11} + (1-c)\left(2g_I + \bar{\lambda}_2h_J\right)\right]\right\}\sin(\bar{\psi}^{(2)}) + 2e_{13}\sin^2(\bar{\psi}^{(2)}) = 0, \tag{33}$$

where $e_{ij} = E_{3i}^{11} + E_{31}^{j3}$ and $f_i = E_{13}^{ii} - E_{31}^{ii}$, with $i,j = 1,2,3$.

For given loading parameters $\bar{\lambda}_1$, $\bar{\lambda}_2$, and $\bar{\theta}$, and material functions g and h, the calculation of the effective stored-energy (31) and the associated particle rotation in (33) require in turn the computation of the appropriate components of the tensor $\mathbf{E}$, as described by

expression (A1) in Appendix A. The pivotal point in this procedure is the calculation of the microstructural tensors $\mathbf{P}_r$, $r = 1,2,3$, as defined by the integrals in (A7). For the general matrix behavior (21), and general choice of $\bar{\lambda}_1$ and $\bar{\lambda}_2$, and $\bar{\theta}$, the analytic calculation of these integrals is a difficult task, and we must resort to the use of a Gaussian quadrature technique. To maintain continuity here, the details are provided in Appendix B.

At this point, it is important to emphasize that expressions (31) and (33) for the macroscopic response of the reinforced elastomers are exactly consistent with the earlier, corresponding expressions given in [4], except that a slightly different form will be used here for the term $h(J)$ in equation (21) defining the matrix behavior $W_\mu^{(1)}$. However, it can be shown that the modifications proposed in this work for the function $h(J)$, as made explicit in the context of expressions (22) and (23) for Gent and neo-Hookean elastomers, respectively, only affect the term $W_\mu^{(1)}(\bar{\mathbf{F}}^{(1)})$ in expression (31), all other terms in expressions (31) and (33) remaining the same. (This is because the other terms in these expressions depend only on up to quadratic terms in the Taylor series expansion of h about $J = 1$.)

Finally, we note that, for the special case of *aligned* loadings, in which stretching directions of the tensor $\bar{\mathbf{U}}$ are aligned with the principal axes of spheroidal particles (in the undeformed configuration), leading to orthotropic symmetry, the calculation of the tensors $\mathbf{P}_r$, and subsequently the corresponding function $\widehat{\Phi}$, can be carried out analytically for special forms of the matrix stored-energy function (21). For this reason, we present in the next subsection explicit analytical results for aligned loadings.

4.2. *Estimates for aligned loadings*

In this subsection, we restrict our attention to the special case of macroscopic loadings aligned with the particle axes $\{\mathbf{e}_i\}$, and characterized by the conditions $\bar{\theta} = 0^\circ$ and $\bar{\theta} = 90^\circ$ in expression (24) (recall that $\bar{\theta}_1 = 0^\circ$). However, for general values of $\bar{\lambda}_1$ and $\bar{\lambda}_2$, it suffices to identify aligned loadings by the condition $\bar{\theta} = 0^\circ$. Hence, the macroscopic deformation gradient for aligned loadings is written as

$$\bar{\mathbf{F}} = \bar{\lambda}_1\, \mathbf{e}_1 \otimes \mathbf{e}_1 + \bar{\lambda}_2\, \mathbf{e}_2 \otimes \mathbf{e}_2 + \left(\bar{\lambda}_1 \bar{\lambda}_2\right)^{-1} \mathbf{e}_3 \otimes \mathbf{e}_3, \tag{34}$$

where it is recalled that the particles are aligned in the $\mathbf{e}_3$ direction.

For the special case of aligned loadings, i.e., $\bar{\theta} = 0^\circ$, it can be shown that $\bar{\psi}^{(2)} = 0$ satisfies identically equation (33), implying that the particles do not rotate for any stretch (up to the possible onset of an instability). Making use of this fact, it is easy to show that the TSO estimate (13) for the effective stored-energy function reduces to

$$\begin{aligned}\widehat{W}(\bar{\mathbf{F}}) = \widehat{\phi}(\bar{\lambda}_1, \bar{\lambda}_2, 0) = (1-c) W_\mu^{(1)}(\bar{\mathbf{F}}^{(1)}) + \frac{c}{2(1-c)} \big\{ (\bar{\lambda}_1 - 1)^2 E_{11}^{11} + (\bar{\lambda}_2 - 1)^2 E_{22}^{22} \\ + l^2 E_{33}^{33} + 2 \big\{ l\,(\bar{\lambda}_1 - 1) E_{33}^{11} + (\bar{\lambda}_2 - 1) \left[(\bar{\lambda}_1 - 1) E_{22}^{11} + l\, E_{33}^{22} \right] \big\} \big\},\end{aligned} \tag{35}$$

where $l = \left(\bar{\lambda}_1 \bar{\lambda}_2\right)^{-1} - 1$, and $W_\mu^{(1)}(\bar{\mathbf{F}}^{(1)}) = g(\bar{I}^{(1)}) + h(\bar{J}^{(1)})$, in which

$$\bar{I}^{(1)} = \frac{(\bar{\lambda}_1 - c)^2 + (\bar{\lambda}_2 - c)^2 + [(\bar{\lambda}_1 \bar{\lambda}_2)^{-1} - c]^2}{(1-c)^2}, \quad \bar{J}^{(1)} = \frac{(\bar{\lambda}_1 - c)(\bar{\lambda}_2 - c)[(\bar{\lambda}_1 \bar{\lambda}_2)^{-1} - c]}{(1-c)^3}. \tag{36}$$

For the general matrix behavior (21), the analytic calculation of the relevant components of tensor $\mathbf{E}$ in (35) is cumbersome, and, for practical reasons, we make use of the Gaussian quadrature technique as will be discussed in Appendix B. However, for some particular types of the matrix behavior (21), and under loading condition (34), derivation of closed-form expressions for the components of the tensor $\mathbf{E}$ and, subsequently, for the

effective stored-energy function (35) is feasible. In the next subsection, we specialize the estimate (35) to neo-Hookean behavior for the matrix phase, and derive closed-form expressions for the effective stored-energy function for the two particular cases of (aligned) *axisymmetric shear* and *pure shear* loadings.

4.2.1. Closed-form results for a neo-Hookean matrix

In this section, we consider the hyperelastic composites made of a neo-Hookean matrix phase with stored-energy function of the form (23) and aligned, spheroidal, rigid particles subjected to aligned loadings of the form (34). Under this type of loading conditions, the TSO estimate (13) for the effective stored-energy function of the composites still takes the form (35) with the function $W_\mu^{(1)}(\bar{\mathbf{F}}^{(1)})$ now given by

$$W_\mu^{(1)}(\bar{\mathbf{F}}^{(1)}) = \frac{1}{2}\mu^{(1)}\left(\bar{I}^{(1)}-3\right)+\frac{1}{2}\mu^{(1)}\left(\bar{J}^{(1)}-1\right)\left(\bar{J}^{(1)}-3\right), \tag{37}$$

where $\bar{I}^{(1)}$ and $\bar{J}^{(1)}$ are given by expressions (36). Note that $W_\mu^{(1)}(\bar{\mathbf{F}}^{(1)})$ remains bounded for all finite values of the stretches. This is different from the corresponding expression originally given in [4] which tends to blow up at a finite value of the stretch depending on the particle volume fraction—a phenomenon that was labeled *geometric* locking up. In other words, the slightly modified expressions given here for the response of the matrix phase lead to no *geometric* locking up. As we will see in Part II of this work, this feature will lead to more accurate predictions for the overall response of the reinforced elastomers.

As discussed earlier, in this case, the microstructural tensors $\mathbf{P}_r, r = 1,2,3$, as defined by integrals (A7), and subsequently the tensor $\mathbf{E}$, as defined by (A1), can be computed analytically for general values of $\bar{\lambda}_1$ and $\bar{\lambda}_2$. However, the expressions for the pertinent components of $\mathbf{E}$, as well as for the final expression for the effective stored-energy function, are too cumbersome to be included here. Instead, we provide only the analytical expressions for the relevant components of the corresponding tensors $\mathbf{P}_r, r = 1,2,3$, although, to maintain continuity here, they are spelled out in Appendix C. Having these components for the tensors $\mathbf{P}_r$, one can conveniently obtain a closed-form expression for the corresponding effective stored-energy function $\widehat{W}$ by first determining the analytic expressions for the relevant components of the tensor $\mathbf{E}$ using the algebraic operations outlined in Eqs. (A1)-(A5), and then substituting these components along with Eq. (37) into Eq. (35). Here, we remark that the resulting expression for the effective stored-energy function simplifies considerably, when specialized to particular choices of $\bar{\lambda}_1$ and $\bar{\lambda}_2$, corresponding to (aligned) *axisymmetric shear* and *pure shear* loadings. In the remainder of this subsection, we will separately consider these two specializations, and provide the closed-form expressions for the associated effective stored-energy functions.

Axisymmetric shear loading. Here, we consider the case of the particle-reinforced neo-Hookean composite subjected to aligned axisymmetric loading of the form (see Fig. 4(a))

$$\bar{\mathbf{F}} = \bar{\lambda}\,\mathbf{e}_1\otimes\mathbf{e}_1+\bar{\lambda}\,\mathbf{e}_2\otimes\mathbf{e}_2+\bar{\lambda}^{-2}\mathbf{e}_3\otimes\mathbf{e}_3, \tag{38}$$

for which $\bar{\lambda}_1 = \bar{\lambda}_2 = \bar{\lambda}$ is a positive loading parameter. In this case, it can be shown that the effective stored-energy function (35) simplifies to

$$\begin{aligned}\widehat{W}(\bar{\mathbf{F}}) = \widehat{\phi}(\bar{\lambda},\bar{\lambda},0) &= (1-c)W_\mu^{(1)}(\bar{\mathbf{F}}^{(1)})\\ &+\frac{c}{2(1-c)}\left\{2(\bar{\lambda}-1)^2E_{11}^{11}+(\bar{\lambda}^{-2}-1)^2E_{33}^{33}+2[(\bar{\lambda}-1)^2E_{22}^{11}+2(\bar{\lambda}^{-2}-1)(\bar{\lambda}-1)E_{33}^{11}]\right\},\end{aligned} \tag{39}$$

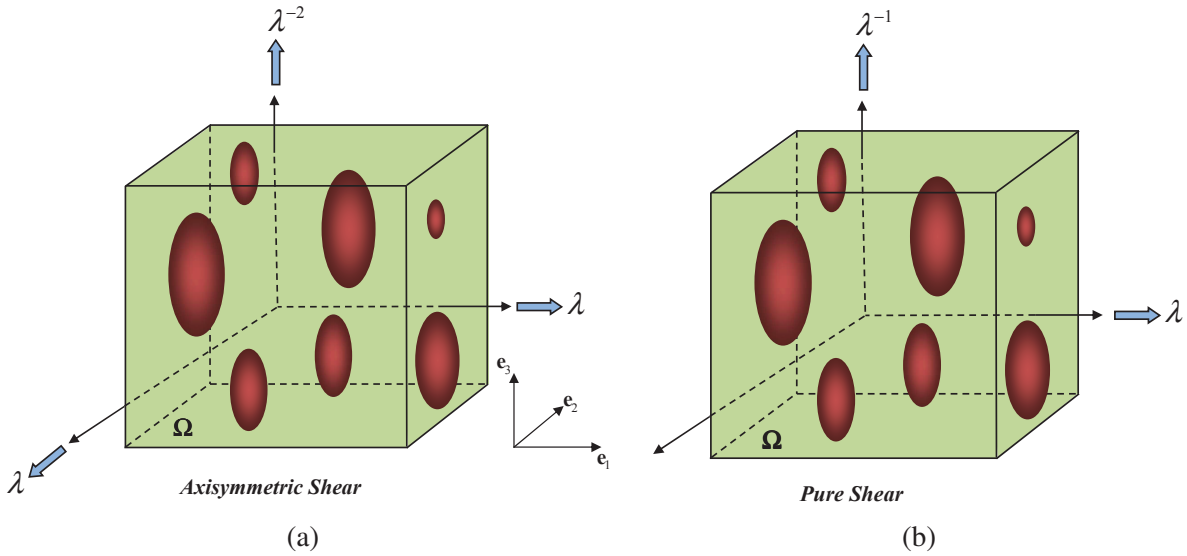

Figure 4. Schematic representation of a matrix reinforced by spheroidal particles subjected to aligned (a) axisymmetric shear loading, (b) pure shear loading.

where $W_\mu^{(1)}$ is given by expression (37) with

$$\bar{I}^{(1)} = \frac{2\,(\bar{\lambda}-c)^2+(\bar{\lambda}^{-2}-c)^2}{(1-c)^2}, \quad \bar{J}^{(1)} = \frac{(\bar{\lambda}-c)^2(\bar{\lambda}^{-2}-c)}{(1-c)^3}.$$

and

$$E_{11}^{11} = A_3A_4A_5(w\gamma_1)^{-1}\Big\{wA_1^2A_3^3(A_3-wA_2)\mathrm{I}_{\bar{1}}^2 - w\bar{\lambda}^{12}A_2^2A_4^4 - wA_3^2A_4^2A_5[2w^4-w^2\mathrm{I}_3^2+4\bar{\lambda}^6]$$
$$+\Big\{w^2\bar{\lambda}^{12}A_2^2A_4^2+wA_2A_3A_5\left[w^4+w^2\mathrm{I}_{\bar{1}}^{\bar{3}}-\bar{\lambda}^6\right]-A_3^2[2w^6-w^4\mathrm{I}_3^3+w^2\mathrm{I}_{\bar{1}}^8+\mathrm{I}_{0,0}^{1,\bar{4}}]\Big\}A_1A_4$$
$$+A_2A_3A_4^2[2w^6\bar{\lambda}^6+w^4\mathrm{I}_{1,0}^{\bar{5},\bar{2}}+(7w^2-3)\bar{\lambda}^{12}]\Big\},$$

$$E_{33}^{33} = A_3A_4A_5w\gamma_1^{-1}\Big\{[wA_3-\bar{\lambda}^6A_2]A_1^2A_3^3\mathrm{I}_{\bar{1}}^2+w\bar{\lambda}^6A_2A_4^2\left(wA_3\mathrm{I}_{0,1}^{\bar{3},2}-\bar{\lambda}^{12}A_2A_4^2\right)+w^3A_3^2A_4^2A_5\mathrm{I}_{0,1}^{\bar{2},0}$$
$$+\Big\{\bar{\lambda}^{18}A_2^2A_4^2+2w\bar{\lambda}^6A_2A_3A_5\mathrm{I}_{0,1}^{\bar{2},0}-w^2A_3^2[w^2\mathrm{I}_2^3+\mathrm{I}_{0,0}^{3,\bar{4}}]\Big\}A_1A_4\Big\},$$

$$E_{22}^{11} = A_3A_4(w\bar{\lambda}^2\gamma_1)^{-1}\Big\{A_1\Big\{-w\bar{\lambda}^2A_2A_3A_4\left[\left(\mathrm{J}_3^{\bar{1}}+\mathrm{I}_{\bar{1},0}^{1,2}\right)w^4-\mathrm{I}_{\bar{1}}^3\left(\mathrm{J}_1^1+\mathrm{I}_{\bar{1}}^3\right)w^2+\bar{\lambda}^6\left(\mathrm{J}_3^{\bar{1}}+\mathrm{I}_{1,0}^{\bar{3},4}\right)\right]$$
$$+A_3^2A_4A_5\left[(\bar{\lambda}^2-1)w^6+\left(\mathrm{I}_{\bar{1}}^5-2\bar{\lambda}^2\right)w^4-\bar{\lambda}^2\left(\mathrm{J}_4^{\bar{1}}-\mathrm{I}_1^1\right)w^2-\bar{\lambda}^8\right]+w^2\bar{\lambda}^{14}A_2^2A_4^3A_5\Big\}$$
$$-\bar{\lambda}^2A_2A_3A_4^2A_5\left[\bar{\lambda}^4(\bar{\lambda}^2-1)w^6+(\bar{\lambda}^2+1)\left(\mathrm{J}_{1,2}^{0,1}-\mathrm{I}_{\bar{1}}^2\right)w^4-\bar{\lambda}^6\left(3\bar{\lambda}^4+\mathrm{I}_{\bar{4}}^2\right)w^2-\bar{\lambda}^{12}\right]$$
$$+w^3A_3^2A_4^2A_5^2[(\bar{\lambda}^2-1)w^2+\bar{\lambda}^2(2\bar{\lambda}^4-1)]+w\bar{\lambda}^{14}A_2^2A_4^4\left[\bar{\lambda}^4(\bar{\lambda}^2+1)w^2+\mathrm{I}_{\bar{1}}^{\bar{2}}-\bar{\lambda}^4\right]$$
$$+wA_1^2A_3^3(2\bar{\lambda}^6-1)\left\{A_3[(\bar{\lambda}^2+1)w^2-\bar{\lambda}^2q_1]-w\bar{\lambda}^2A_2A_5\right\}\Big\},$$

$$E_{33}^{11} = -A_3A_4\bar{\lambda}\gamma_1^{-1}\Big\{A_1\Big\{wA_3^2A_4A_5\left[(\bar{\lambda}^2+1)w^4-w^2\left(\mathrm{J}_{0,2}^{0,1}+\mathrm{I}_{\bar{1}}^5\right)+\mathrm{I}_{0,0}^{\bar{1},4}+2\bar{\lambda}^8\right]-w\bar{\lambda}^{14}A_2^2A_4^3A_5$$
$$+\bar{\lambda}^2A_2A_3A_4\left[w^4\left(\mathrm{J}_3^{\bar{1}}+\mathrm{I}_{\bar{2}}^4\right)+\bar{\lambda}^4\left(2\bar{\lambda}^{14}+\mathrm{J}_{0,\overline{10}}^{0,4}-\mathrm{I}_{\bar{1},0}^{2,3}\right)w^2+2\bar{\lambda}^{18}+\bar{\lambda}^{10}\mathrm{I}_{\bar{1}}^3\right]\Big\}$$
$$-\bar{\lambda}^{14}A_2^2A_4^4(w^2q_1-\bar{\lambda}^6-\bar{\lambda}^4)-w\bar{\lambda}^2A_2A_3A_4^2A_5\left[w^4q_1-\left(\mathrm{J}_3^1+3\bar{\lambda}^6\right)w^2+2\bar{\lambda}^{12}+3\bar{\lambda}^{10}\right]$$
$$+w^2A_3^2A_4^2A_5^2\mathrm{I}_{0,1}^{\bar{2},0}+A_1^2A_3^3\mathrm{I}_{\bar{1}}^2\left\{w\bar{\lambda}^2A_2A_5-A_3[(\bar{\lambda}^2+1)w^2-\bar{\lambda}^2q_1]\right\}\Big\}. \qquad (40)$$

In addition, in the above relations,

$$A_1=\tanh^{-1}\left(\frac{\sqrt{w^2-1}}{w}\right),\ A_2=\tanh^{-1}\left(\frac{\sqrt{w^2-\bar{\lambda}^6}}{w}\right),\ A_3=\sqrt{w^2-\bar{\lambda}^6},$$
$$A_4=\sqrt{w^2-1},\ \ A_5=(\bar{\lambda}^4+\bar{\lambda}^2+1)(\bar{\lambda}^2-1),\ \ q_{1,2}=\bar{\lambda}^4\pm1,$$
$$\gamma_1=A_3A_4\Big[A_1A_3A_4\left(\bar{\lambda}^6A_2A_3^2A_4^2\mathrm{I}_{\bar{1}}^3+wA_3^3A_5\mathrm{I}_{1,1}^{\bar{4},0}\right)-A_1^2A_3^6\mathrm{I}_{\bar{1}}^2-\bar{\lambda}^{18}A_2^2A_4^6$$
$$-w\bar{\lambda}^6A_2A_3A_4^4A_5\mathrm{I}_{0,1}^{\bar{3},0}+w^2A_3^2A_4^2A_5^2\mathrm{I}_{0,1}^{\bar{2},0}\Big]/\mu^{(1)},$$

and the abbreviations

$$\mathrm{I}^{a,c}_{b,d} = c\bar{\lambda}^{12} + a\bar{\lambda}^{6} + d\,w^2 + b,\ \ \mathrm{I}^{a}_{b} = \mathrm{I}^{a,0}_{b,0},\ \ \mathrm{J}^{a,c}_{b,d} = b\bar{\lambda}^{10} + d\bar{\lambda}^{8} + a\bar{\lambda}^{4} + c\bar{\lambda}^{2},\ \ \mathrm{J}^{a}_{b} = \mathrm{J}^{a,0}_{b,0},$$

have been introduced for compactness. In these last expressions, a barred subscript/superscript indicates the corresponding negative coefficient. It should be pointed out that the effective stored-energy function (39) is valid for both prolate ($w > 1$) and oblate ($w < 1$) spheroidal shapes for the particles. Also, when specialized to the case of $w = 1$, relation (39) recovers the corresponding effective stored-energy function for neo-Hookean elastomers reinforced by rigid, spherical particles provided by relation (141) in [4] (except that the expression for $W^{(1)}_{\mu}$ involves a logarithmic term in $\bar{J}^{(1)}$, because, as already noted, a slightly different form for the compressible generalization of the neo-Hookean model was used in the earlier work.). Another remarkable feature of the stored-energy function (39) is that it is valid for any positive loading parameter $\bar{\lambda}$. More specifically, for $\bar{\lambda} > 1$, the function (39) corresponds to the effective stored-energy function of the composite when subjected to *Equibiaxial Tension* loading in the $\mathbf{e}_1 - \mathbf{e}_2$ plane, while for $\bar{\lambda} < 1$, it corresponds to *Uniaxial Tension* loading in the $\mathbf{e}_3$ direction with tensile stretch $\bar{\lambda}_3 = 1/\bar{\lambda}^2$.

Pure shear loading. Next, we consider the case in which the (spheroidal) particle-reinforced neo-Hookean composite undergoes aligned pure shear loading (in the $\mathbf{e}_1 - \mathbf{e}_3$ plane) of the form (see Fig. 4(b))

$$\bar{\mathbf{F}} = \bar{\lambda}\,\mathbf{e}_1 \otimes \mathbf{e}_1 + \mathbf{e}_2 \otimes \mathbf{e}_2 + \bar{\lambda}^{-1}\,\mathbf{e}_3 \otimes \mathbf{e}_3, \tag{41}$$

where, similar to the preceding axisymmetric case, $\bar{\lambda}_1 = \bar{\lambda}$ is a positive loading parameter. In this case, the TSO estimate (35) for the effective stored-energy function simplifies to

$$\begin{aligned}\widehat{W}(\bar{\mathbf{F}}) = \widehat{\phi}(\bar{\lambda},1,0) = (1-c)W^{(1)}_{\mu}(\bar{\mathbf{F}}^{(1)}) + \frac{c}{2(1-c)}\big\{&(\bar{\lambda}-1)^2E^{11}_{11} + (\bar{\lambda}^{-1}-1)^2E^{33}_{33}\\ &+ 2\,(\bar{\lambda}-1)\,(\bar{\lambda}^{-1}-1)E^{11}_{33}\big\},\end{aligned} \tag{42}$$

where $W^{(1)}_{\mu}$ is given by expression (37) with

$$\bar{I}^{(1)} = \frac{(\bar{\lambda}-c)^2 + (\bar{\lambda}^{-1}-c)^2}{(1-c)^2} + 1, \quad \bar{J}^{(1)} = \frac{(\bar{\lambda}-c)(\bar{\lambda}^{-1}-c)}{(1-c)^2},$$

and

$$\begin{aligned}E^{11}_{11} = -(w\bar{\lambda}\,\gamma_2)^{-1}\mathrm{Q}^1_{\bar{1}}\Big\{&w\bar{\lambda}\,B_2B_3^2\left(wB_3^2\Xi_{p2} - \bar{\lambda}\,B_2^3\right)\left[wB_1\,\mathrm{Q}^1_2 + B_3\left(\bar{\lambda}^2w^2 - 2\,\mathrm{Q}^1_{\bar{1}}\right)\right]\Xi_{p1}\\
&- wB_2^2B_3^2\,\mathrm{Q}^1_{\bar{1}}\left[w^2B_1^2B_3\,\mathrm{Q}^1_{\bar{1}} - w\left(w^4\mathrm{Q}^1_{\bar{1}} - 4\,\bar{\lambda}^2w^2 + \mathrm{O}^{1,1}_{1,1}\right)B_1 + \left(w^4\mathrm{Q}^1_{\bar{1}} + w^2\mathrm{O}^{1,1}_{\bar{3},\bar{1}} + 2\,\bar{\lambda}^6\right)B_3\right]\Xi_{p2}\\
&+ \Big\{w^2\,\bar{\lambda}\,q_2B_2B_3^2\left[wB_1\,\mathrm{Q}^1_2 + \left(\bar{\lambda}^2w^2 - 2\mathrm{Q}^1_{\bar{1}}\right)B_3\right]\Xi_{p1} - w^2\,\bar{\lambda}\,B_2^3B_3^2\left[wB_1\,\mathrm{Q}^1_2 + \left(\bar{\lambda}^2w^2 - 2\mathrm{Q}^1_{\bar{1}}\right)B_3\right]\Xi_{p2}\\
&- wB_2^2\left[w^2q_2^3B_1^2B_3 + wB_1B_3^2\left(w^2\mathrm{O}^{1,\bar{1},1}_{2,0,0} + \mathrm{O}^{1,1,\bar{3}}_{2,\bar{4},0}\right) + B_3^3\left(w^4\bar{\lambda}^4 - w^2\mathrm{O}^{1,1,1}_{2,0,0} + 2\,\bar{\lambda}^6\mathrm{Q}^1_{\bar{1}}\right)\right]\Big\}\Xi_f\\
&+ \bar{\lambda}B_2^5\,\mathrm{Q}^1_{\bar{1}}\left[w^2B_1^2B_3\,\mathrm{Q}^1_{\bar{1}} + wB_1B_3^2\left(w^2\mathrm{Q}^1_{\bar{1}} - \mathrm{Q}^3_{\bar{1}}\right) - B_3^3\left(w^2\mathrm{Q}^1_{\bar{1}} - 2\,\bar{\lambda}^2\right)\right]\Big\},\end{aligned}$$

$$E_{33}^{33}=-w\gamma_2^{-1}\mathrm{Q}_{\bar{1}}^{1}\Bigg\{\bar{\lambda}\left(B_1-wB_3\right)B_2B_3^2\,\mathrm{Q}_2^1\left(w\bar{\lambda}^{\,3}B_3^2\,\Xi_{p2}-B_2^3\right)\Xi_{p1}-w\bar{\lambda}\,B_2^2B_3^2\,\mathrm{Q}_1^1\left\{\bar{\lambda}^{\,2}B_{\bar{1}}^2B_3\,\mathrm{Q}_1^1\right.$$
$$\left.+w\,\alpha B_1-w^2B_3\left(2w^2-\bar{\lambda}^{\,2}\mathrm{Q}_1^1\right)\right\}\Xi_{p2}+\bar{\lambda}^{\,3}\Big\{w\bar{\lambda}\,B_2B_3^2\left(B_1-wB_3\right)\left(B_4\,\mathrm{Q}_1^1\,\Xi_{p1}-B_2^2\,\mathrm{Q}_2^1\,\Xi_{p2}\right)$$
$$-B_2^2\left[wq_2^3B_{\bar{1}}^2B_3-B_1B_3^2\left(w^2\mathrm{O}_{\bar{4},2,0}^{\bar{2},0,1}+\bar{\lambda}^{\,6}\mathrm{Q}_2^1\right)-wB_3^3\left(w^2\mathrm{Q}_1^2-\bar{\lambda}^{\,6}\mathrm{Q}_2^1\right)\right]\Big\}\,\Xi_f$$
$$\left.+B_2^5B_3\left(\bar{\lambda}^{\,2}+1\right)^2\left(B_1-wB_3\right)^2\right\},$$

$$E_{33}^{11}=\gamma_2^{-1}\Bigg\{\bar{\lambda}\,B_3^2\Big\{B_2^4\left[\left(w^2\,\bar{\lambda}^{\,2}\mathrm{Q}_3^1-2\mathrm{Q}_1^1\right)B_3-wB_1B_4\right]-w\bar{\lambda}\,B_2B_3^2\left(wB_1B_4+\alpha B_3\right)\Xi_{p2}\Big\}\Xi_{p1}$$
$$+w\bar{\lambda}\,q_2B_2^2B_3^2\left[wB_{\bar{1}}^2B_3\,\mathrm{Q}_1^1+\left(w^4\mathrm{Q}_{\bar{1}}^{\bar{1}}+w^2\mathrm{Q}_{\bar{1}}^1+\bar{\lambda}^{\,2}\mathrm{Q}_1^1\right)B_1+w\left(2w^2-\bar{\lambda}^{\,2}\mathrm{Q}_1^1\right)B_3\right]\Xi_{p2}$$
$$+\bar{\lambda}\left\{B_2^2\left[w^2B_3\,q_2^2\mathrm{Q}_1^1B_{\bar{1}}^2+B_3^3\left(w^4\mathrm{O}_{2,1,0}^{1,0,0}-w^2\mathrm{O}_{1,3,1}^{0,2,1}+2\bar{\lambda}^{\,8}\mathrm{Q}_1^1\right)+wB_3^2\,\mathrm{Q}_{\bar{1}}^1\left(w^2\mathrm{O}_{5,2,0}^{2,3,1}-\mathrm{O}_{1,6,0}^{0,3,3}\right)B_1\right]\right.$$
$$\left.-w\bar{\lambda}\,B_2B_3^2\left(wB_1B_4+\alpha B_3\right)\left(q_2\,\Xi_{p1}-B_2^2\,\Xi_{p2}\right)\right\}\Xi_f+q_2^2B_2^5\left(wB_{\bar{1}}^2B_3+\left(w^4-1\right)B_1+wB_3^3\right)\Bigg\}. \tag{43}$$

In addition, in the above relations,

$$B_1=\tan^{-1}\left(\frac{\sqrt{1-w^2}}{w}\right),\quad B_2=\sqrt{\bar{\lambda}^{\,4}-w^2},\quad B_3=\sqrt{1-w^2},\quad B_4=(\bar{\lambda}^{\,2}-1)(\bar{\lambda}^{\,2}+2),$$

$$\gamma_2=\Bigg\{\bar{\lambda}\,B_3^2\left\{2w\bar{\lambda}^{\,3}B_2B_3^5\,\Xi_{p2}-B_2^4\left[wB_1B_4-B_3\left(w^2\bar{\lambda}^{\,2}\mathrm{Q}_1^1-2\right)\right]\right\}\Xi_{p1}+q_2B_2^5\,\mathrm{Q}_1^1\left[wB_{\bar{1}}^2B_3\right.$$
$$\left.+(w^4-1)B_1-w^3B_3+wB_3\right]+w\bar{\lambda}\,q_2B_2^2B_3^2\Big[w\left(2w^2-\bar{\lambda}^{\,2}\mathrm{Q}_1^1\right)B_3-\left(2w^4-\bar{\lambda}^{\,2}\mathrm{Q}_1^1\right)B_1\Big]\Xi_{p2}$$
$$+\bar{\lambda}^{\,3}B_3^4\left\{2w\bar{\lambda}\,B_2B_3\left(q_2\,\Xi_{p1}-B_2^2\,\Xi_{p2}\right)-B_2^2\left[wB_1\,\mathrm{Q}_{\bar{1}}^1\,\mathrm{O}_{2,0}^{1,2}+B_3\left(w^2\mathrm{Q}_1^1-2\,\bar{\lambda}^{\,6}\right)\right]\right\}\Xi_f\Bigg\}/\mu^{(1)}$$

and $\alpha=w^2\left(\bar{\lambda}^{\,2}\mathrm{Q}_1^1+2\right)-2\bar{\lambda}^{\,2}\mathrm{Q}_1^1$. Also, the abbreviations

$$\mathrm{Q}_b^a=a\bar{\lambda}^{\,2}+b,\quad \mathrm{O}_{b,d,f}^{a,c,e}=f\bar{\lambda}^{\,10}+e\bar{\lambda}^{\,8}+d\bar{\lambda}^{\,6}+c\bar{\lambda}^{\,4}+b\bar{\lambda}^{\,2}+a,\quad \mathrm{O}_{b,d}^{a,c}=\mathrm{O}_{b,d,0}^{a,c,0},$$

are introduced for compactness, and it is recalled that a barred subscript/superscript indicates the corresponding negative coefficient. Moreover, Ξ_f, and $\Xi_{p1,2}$ are given in terms of the incomplete elliptic integrals of the first and third kind [1], respectively, via

$$\Xi_f=F\left(\frac{B_2}{\bar{\lambda}^{\,2}},q\right),\ \Xi_{p1}=P\left(\frac{B_2}{\bar{\lambda}^{\,2}},\frac{\bar{\lambda}^{\,4}-1}{w^2-\bar{\lambda}^{\,4}},q\right),\ \Xi_{p2}=P\left(\frac{B_2}{\bar{\lambda}^{\,2}},1,q\right),$$

where $q=\bar{\lambda}\sqrt{(\bar{\lambda}^2-1)/(\bar{\lambda}^4-w^2)}$, and the functions F and P are defined by

$$F(a,b)=\int_0^a \frac{1}{\sqrt{1-t^2}\sqrt{1-b^2t^2}}dt, \quad P(a,b,c)=\int_0^a \frac{1}{\sqrt{1-t^2}\sqrt{1-bt^2}\sqrt{1-c^2t^2}}dt. \tag{44}$$

It is important to note that, similar to relation (39), the effective stored-energy function (42) is valid for both prolate ($w>1$) and oblate ($w<1$) spheroidal shapes of particles. Likewise, when specialized to the case of $w=1$, relation (42) reduces to the corresponding effective stored-energy function for neo-Hookean elastomers reinforced by rigid, spherical particles provided by relation (139) in [4] (notwithstanding the earlier comment about the logarithmic term). Finally, it is emphasized, for completeness, that the estimates (39) and (42) are consistent with the macroscopic incompressibility constraint $\bar{\lambda}_1\bar{\lambda}_2\bar{\lambda}_3=1$, and linearize properly.

5. Onset of macroscopic instabilities

The purpose of this section is to investigate the possible development of macroscopic instabilities in the finitely strained, particle-reinforced elastomers described in the prior section. As discussed earlier in Section 2, in this work, our attention is restricted to the onset of *macroscopic* (as opposed to *microscopic*) instabilities, which are characterized by wavelengths much larger than the characteristic size of the underlying microstructure. We recall from our discussion in Section 2 that, based on the work by Geymonat et al. [14], the onset of macroscopic instabilities in the heterogeneous materials corresponds to the loss of strong ellipticity of the associated homogenized constitutive behavior. Recalling from (11), the homogenized particle-reinforced elastomer characterized by $\widehat{W}(\bar{\mathbf{F}})$ is said to be strongly elliptic if and only if

$$\widehat{L}_{ijkl}N_jN_l\,m_im_k=\left(\partial^2\widehat{W}/\partial\bar{F}_{ij}\,\partial\bar{F}_{kl}N_jN_l\right)m_im_k>0. \tag{45}$$

Thus, equivalently, the *first* macroscopic instability happens whenever the inequality (45) ceases to hold true.

For incompressible materials, however, it proves convenient to express the strong ellipticity (SE) condition in terms of the tensor $\widehat{L}^c_{ijkl}=\widehat{L}_{ipkq}\bar{F}_{jp}\bar{F}_{lq}$ which is the updated incremental moduli tensor when the undeformed configuration coincides with the deformed configuration. Correspondingly, for incompressible composites, the SE condition (45) can be rewritten as

$$\mathrm{tr}\{[\widehat{\mathbf{L}}^c(\mathbf{m}\otimes\mathbf{n})](\mathbf{m}\otimes\mathbf{n})\}>0, \tag{46}$$

where $\mathbf{n}=\bar{\mathbf{F}}^{-T}\mathbf{N}$ is the transformation of the unit vector $\mathbf{N}$ in the deformed configuration. In this case, the incompressibility constraint $\det(\bar{\mathbf{F}})=1$ implies that the unit vectors $\mathbf{n}$ and $\mathbf{m}$ must satisfy $\mathbf{n}\cdot\mathbf{m}=0$ in (46). In fact, due to the incompressibility constraint, some components of the moduli $\mathbf{L}^c$ become infinite, however, the constraint $\mathbf{n}\cdot\mathbf{m}=0$ projects the tensor $\mathbf{L}^c$ onto the space of isochoric deformation $\det(\bar{\mathbf{F}})=1$, and accordingly, the condition (46) is expressed in terms of some traces of $\mathbf{L}^c$ with finite values.

Since the effective strain energy (13) is strongly elliptic in sufficiently small neighborhoods of $\bar{\mathbf{F}}=\mathbf{I}$, one expects that the inequality (46) holds true in the infinitesimal-strain regime. However, as the macroscopic strain increases, the inequality may be violated at some specific critical tensor $\bar{\mathbf{F}}^{cr}$. This critical deformation gradient is associated with the critical vectors $\mathbf{n}_{cr}$, $\mathbf{m}_{cr}$. In fact, $\bar{\mathbf{F}}^{cr}$ constitutes the boundary of the domain in deformation space, including the value $\bar{\mathbf{F}}=\mathbf{I}$, inside which the SE condition holds. It is also remarked

that when the condition (46) fails to hold, the homogenized material becomes macroscopically unstable and this corresponds to a developing *shear band* taking place on a plane with the (unit) normal vector $\mathbf{n}_{cr}$ (in the deformed configuration) and along the direction $\mathbf{m}_{cr}$.

The main objective of this section is to find the $\bar{\mathbf{F}}^{cr}$ (together with the associated vectors $\mathbf{n}_{cr}$ and $\mathbf{m}_{cr}$) when the composite material consisting of rigid spheroidal particles undergoes the macroscopic deformation given by (24). In the following, the specialization of the SE condition (46) for the class of *transversely isotropic* composites under non-aligned and aligned loadings are provided, and later, they are further specialized for the (rigidly) particle-reinforced composites of interest under axisymmetric and pure shear loadings.

The modulus tensor $\widehat{\mathbf{L}}^c$ in (46), which in general has 45 independent components, simplifies when it is specialized to the class of (incompressible) transversely isotropic composites (with symmetry axis aligned with $\mathbf{e}_3$ direction) undergoing the macroscopic deformation field (24) (recall that $\bar{\theta}_1 = 0^\circ$). Accordingly, it can be shown, by making use of the orthogonality condition $\mathbf{n}\cdot\mathbf{m} = 0$ to solve for m_3 in terms of the other components of $\mathbf{m}$ and $\mathbf{n}$, that the SE condition (46) for the stored-energy function $\widehat{W}(\bar{\mathbf{F}})$ can be written as

$$
\begin{aligned}
& n_3^{-2}\Bigg\{ \Big\{\widehat{L}^c_{3131}\,n_1^4 - 2\widehat{L}^*_2\,n_3 n_1^3 + \Big(\widehat{L}^c_{3232}\,n_2^2 + \widehat{L}^*_3\,n_3^2\Big)\,n_1^2 + \Big(2\widehat{L}^*_1\,n_3^3 - 2\widehat{L}^c_{3212}\,n_2^2\,n_3\Big)\,n_1 + \\
& \widehat{L}^c_{1212}\,n_2^2 n_3^2 + \widehat{L}^c_{1313}\,n_3^4\Big\}\,m_1^2 + \Big\{2\widehat{L}^c_{3131}\,n_2\,n_1^3 + 2\Big(\widehat{L}^*_7\,n_3^2 - \widehat{L}^*_8\,n_1^2 - \widehat{L}^c_{3212}\,n_2^2\Big)\,n_2\,n_3 \\
& + 2\Big(\widehat{L}^c_{3232}\,n_2^2 + \widehat{L}^*_5\,n_3^2\Big)\,n_1 n_2\Big\}\,m_1 m_2 + \Big[\Big(\widehat{L}^c_{3131}\,n_2^2 + \widehat{L}^c_{2121}\,n_3^2\Big)\,n_1^2 \\
& + 2\Big(\widehat{L}^c_{2321}\,n_3^2 - \widehat{L}^*_6\,n_2^2\Big)\,n_1 n_3 + \widehat{L}^c_{3232}\,n_2^4 + \widehat{L}^*_4\,n_3^2 n_2^2 + \widehat{L}^c_{2323}\,n_3^4\Big]\,m_2^2\Bigg\} > 0,
\end{aligned}
\tag{47}
$$

where

$$
\begin{aligned}
& \widehat{L}^*_1 = \widehat{L}^c_{1113} - \widehat{L}^c_{3313}, \quad \widehat{L}^*_2 = \widehat{L}^c_{1131} - \widehat{L}^c_{3331}, \\
& \widehat{L}^*_3 = \widehat{L}^c_{1111} + \widehat{L}^c_{3333} - 2\widehat{L}^c_{1133} - 2\widehat{L}^c_{1331}, \quad \widehat{L}^*_4 = \widehat{L}^c_{2222} + \widehat{L}^c_{3333} - 2\widehat{L}^c_{2233} - 2\widehat{L}^c_{2332} \\
& \widehat{L}^*_5 = \widehat{L}^c_{1122} + \widehat{L}^c_{1221} + \widehat{L}^c_{3333} - \widehat{L}^c_{1133} - \widehat{L}^c_{2233} - \widehat{L}^c_{1331} - \widehat{L}^c_{2332}, \\
& \widehat{L}^*_6 = \widehat{L}^c_{2231} + \widehat{L}^c_{3221} - \widehat{L}^{\prime c}_{3331}, \ \widehat{L}^*_7 = \widehat{L}^c_{2213} + \widehat{L}^c_{2312} - \widehat{L}^c_{3313}, \ \widehat{L}^*_8 = \widehat{L}^c_{2231} + \widehat{L}^c_{3221} + \widehat{L}^c_{1131} - 2\widehat{L}^c_{3331},
\end{aligned}
\tag{48}
$$

The loss of strong ellipticity of the (incompressible) composite elastomer can be determined by monitoring the sign of the LHS expression in inequality (47) for all possible unit vectors $\mathbf{n}$ and $\mathbf{m}$ satisfying the constraint $\mathbf{n}\cdot\mathbf{m} = 0$, and detecting the point at which the expression first vanishes. As mentioned earlier in this section, for an incompressible composite, some of the components of the corresponding effective incremental modulus tensor $\widehat{\mathbf{L}}^c$ become unbounded, however, the traces of this modulus tensor which appear in the strong ellipticity condition (47) (the expressions of $\widehat{L}^c_{ijkl}$ terms multiplying n_i's components) have finite values. These traces can be derived in terms of loading parameters $\bar{\lambda}_1$, $\bar{\lambda}_2$, and $\bar{\theta}_2$ as well as the first and second derivatives of the effective stored-energy function $\widehat{\Phi}(\bar{\lambda}_1, \bar{\lambda}_2, \bar{\theta}_1, \bar{\theta}_2)$ with respect to its arguments, evaluated at $\bar{\theta}_1 = 0^\circ$. To maintain continuity, the corresponding explicit expressions for the moduli traces, calculated in the rectangular Cartesian basis $\{\mathbf{e}'_i\}$, are provided in Appendix D.

Substituting the expressions for the moduli traces (in (D2)-(D6)) into (47), the SE condition is expressed in terms of $\widehat{\Phi}$ and can be used to detect the onset of macroscopic instabilities for the class of particle-reinforced composites described in Section 4. For a

general choice of $\bar{\lambda}_1$, $\bar{\lambda}_2$, and $\bar{\theta} = \bar{\theta}_2$ in deformation (24) (recall that $\bar{\theta}_1 = 0^\circ$), the resulting condition takes the form

$$f(\widehat{\Phi}_{,\bar{\lambda}_1}, \widehat{\Phi}_{,\bar{\lambda}_2}, \widehat{\Phi}_{,\bar{\lambda}_1\bar{\lambda}_1}, \widehat{\Phi}_{,\bar{\lambda}_2\bar{\lambda}_2}, \widehat{\Phi}_{,\bar{\theta}_1\bar{\theta}_1}, \widehat{\Phi}_{,\bar{\theta}_2\bar{\theta}_2}, n_1, n_2, n_3, m_1, m_2, m_3, \bar{\lambda}_1, \bar{\lambda}_2, \bar{\theta}) > 0, \qquad (49)$$

in which subscript commas followed by an index denote derivatives with respect to the corresponding variables. For this general choice of loading parameters, the explicit expression for function f in (49) is too lengthy to be included here, but it simplifies considerably for the special case of aligned loadings ($\bar{\theta} = 0^\circ$) as discussed in the following.

For the special case of macroscopic aligned loadings, given by (34), it can be shown that the SE condition (47) reduces to

$$\begin{aligned} & n_3^{-2}\Big\{\Big[\widehat{L}^c_{3131}\, n_1^4 + \Big(\widehat{L}^c_{3232}\, n_2^2 + \widehat{L}^*_3\, n_3^2\Big)\, n_1^2 + \widehat{L}^c_{1313}\, n_3^4 + \widehat{L}^c_{1212}\, n_2^2 n_3^2\Big]\, m_1^2 \\ & + \Big[2\widehat{L}^c_{3131}\, n_1^3 n_2 + \Big(2\widehat{L}^c_{3232}\, n_2^3 + 2\widehat{L}^*_5\, n_2 n_3^2\Big)\, n_1\Big]\, m_1 m_2 \\ & + \Big[\Big(\widehat{L}^c_{2121} n_3^2 + \widehat{L}^c_{3131}\, n_2^2\Big)\, n_1^2 + \widehat{L}^c_{3232}\, n_2^4 + \widehat{L}^*_4\, n_2^2 n_3^2 + \widehat{L}^c_{2323} n_3^4\Big]\, m_2^2\Big\} > 0. \end{aligned} \qquad (50)$$

Substituting the moduli traces in (D7)-(D9) (for aligned loadings) into the above condition, the corresponding SE condition for $\widehat{\Phi}$ is obtained. For general choice of $\bar{\lambda}_1$ and $\bar{\lambda}_2$ in deformation (34), the resulting condition can be shown to reduce to

$$\begin{aligned} & l_1^{-2} l_2^{-2} l_3^{-1} \Bigg\{ \Big\{\bar{\lambda}_1^4 \bar{\lambda}_2^2 l_2^2 l_3 \phi_1^* n_1^4 + \Big[\bar{\lambda}_1^2 \bar{\lambda}_2^4 l_1^2 l_3 \phi_2^* n_2^2 + \bar{\lambda}_1 l_2^2 l_3 \Big(\bar{\lambda}_1 l_1^2 \widehat{\Phi}_{,\bar{\lambda}_1\bar{\lambda}_1} - 2\bar{\lambda}_1^3 \bar{\lambda}_2^2 \widehat{\Phi}_{,\bar{\theta}_2\bar{\theta}_2} - 2 l_1 \widehat{\Phi}_{,\bar{\lambda}_1}\Big) n_3^2\Big] n_1^2 \\ & + \bar{\lambda}_2^2 l_2^2 l_1^2 \phi_3^* n_2^2 n_3^2 + \bar{\lambda}_1 l_2^2 l_3 \Big(l_1 \widehat{\Phi}_{,\bar{\lambda}_1} + \bar{\lambda}_1^3 \bar{\lambda}_2^2 \widehat{\Phi}_{,\bar{\theta}_2\bar{\theta}_2}\Big) n_3^4\Big\} m_1^2 + 2\Big\{\bar{\lambda}_1^4 \bar{\lambda}_2^2 l_2^2 l_3 \phi_1^* n_1^3 n_2 \\ & + \Big\{\Big[\bar{\lambda}_1 \bar{\lambda}_2 l_3 \Big(l_1^2 l_2^2 \widehat{\Phi}_{,\bar{\lambda}_1\bar{\lambda}_2} - \bar{\lambda}_1^3 \bar{\lambda}_2 l_2^2 \widehat{\Phi}_{,\bar{\theta}_2\bar{\theta}_2} - \bar{\lambda}_1 \bar{\lambda}_2^3 l_1^2 \widehat{\Phi}_{,\bar{\theta}_1\bar{\theta}_1}\Big) + l_1 l_2 \Big(\bar{\lambda}_1^3 l_2^2 \widehat{\Phi}_{,\bar{\lambda}_1} - \bar{\lambda}_2^3 l_1^2 \widehat{\Phi}_{,\bar{\lambda}_2}\Big)\Big] n_2 n_3^2 \\ & + \bar{\lambda}_1^2 \bar{\lambda}_2^4 l_1^2 l_3 \phi_2^* n_2^3\Big\} n_1\Big\} m_1 m_2 + \Big\{ \big(\bar{\lambda}_1^4 \bar{\lambda}_2^2 l_2^2 l_3 \phi_1^* n_2^2 + \bar{\lambda}_1^2 l_2^2 l_1^2 \phi_3^* n_3^2\big) n_1^2 + \bar{\lambda}_1^2 \bar{\lambda}_2^4 l_1^2 l_3 \phi_2^* n_2^4 \\ & + \bar{\lambda}_2 l_1^2 l_3 \Big[\Big(\bar{\lambda}_2 l_2^2 \widehat{\Phi}_{,\bar{\lambda}_2\bar{\lambda}_2} - 2\bar{\lambda}_1^2 \bar{\lambda}_2^3 \widehat{\Phi}_{,\bar{\theta}_1\bar{\theta}_1} - 2 l_2 \widehat{\Phi}_{,\bar{\lambda}_2}\Big) n_2^2 n_3^2 + \Big(l_2 \widehat{\Phi}_{,\bar{\lambda}_2} + \bar{\lambda}_1^2 \bar{\lambda}_2^3 \widehat{\Phi}_{,\bar{\theta}_1\bar{\theta}_1}\Big) n_3^4\Big]\Big\} m_2^2\Bigg\}\Bigg|_{\bar{\theta}_1 = 0^\circ} n_3^{-2} > 0, \end{aligned} \qquad (51)$$

where $\phi_1^* = \bar{\lambda}_1 l_1 \widehat{\Phi}_{,\bar{\lambda}_1} + \widehat{\Phi}_{,\bar{\theta}_2\bar{\theta}_2}$, $\phi_2^* = \bar{\lambda}_2 l_2 \widehat{\Phi}_{,\bar{\lambda}_2} + \widehat{\Phi}_{,\bar{\theta}_1\bar{\theta}_1}$, $\phi_3^* = \bar{\lambda}_1 \widehat{\Phi}_{,\bar{\lambda}_1} - \bar{\lambda}_2 \widehat{\Phi}_{,\bar{\lambda}_2}$, and

$$l_1 = \bar{\lambda}_1^4 \bar{\lambda}_2^2 - 1, \quad l_2 = \bar{\lambda}_1^2 \bar{\lambda}_2^4 - 1, \quad l_3 = \bar{\lambda}_1^2 - \bar{\lambda}_2^2. \qquad (52)$$

Before proceeding with the study of conditions (47), (49), (50), (51) for the particle-reinforced composites of interest, it is important to make the following remarks:

(1) The SE conditions (49) and (51) are valid for any stored-energy function of the form $\Phi(\bar{\lambda}_1, \bar{\lambda}_2, \bar{\theta}_1, \bar{\theta}_2)$ corresponding to a transversely isotropic material whose axis of symmetry is aligned with the $\mathbf{e}_3$ direction and subjected to a deformation field of the form (24) (with the condition $\bar{\theta}_1 = 0^\circ$) and (34), respectively.

(2) In the remainder of this section, we will examine the SE conditions (49) and (51) only for the transversely isotropic composite with the class of particulate microstructures studied in this work. For this class of composites, based on a numerical study of (49) and (51) (as will be discussed in Part II of this work), we provide the corresponding critical unit vectors $\mathbf{n}_{cr}$ and $\mathbf{m}_{cr}$ at which these condition are first violated.

(3) The aforementioned results for the critical vectors $\mathbf{n}_{cr}$, $\mathbf{m}_{cr}$ are based on numerical investigations carried out for composites with Gent and neo-Hookean matrices. However, it is plausible that corresponding calculations for composites with other matrix models of the form (21) would result in the same critical unit vectors.

Keeping in mind these remarks, in the next two subsections we consider the strong ellipticity conditions (49) and (51) for two special types of loadings. In the first subsection, we consider *axisymmetric shear* (characterized by $\bar{\lambda}_1 = \bar{\lambda}_2 = \bar{\lambda}$), and provide first the SE conditions associated with expressions (49) and (51) for non-aligned and aligned loadings, respectively. In the second, we provide the corresponding specialized SE conditions for *pure shear* loadings (characterized by $\bar{\lambda}_1 = \bar{\lambda}, \bar{\lambda}_2 = 1$). In this context, it is useful to introduce the critical stretch $\bar{\lambda}_{cr}$, at which the strong ellipticity conditions associated with axisymmetric and pure shear loadings are first violated.

In the discussions below, it is helpful to introduce the notations

$$\widehat{\Phi}^{AS}(\bar{\lambda}, \bar{\theta}_1, \bar{\theta}_2) = \widehat{\Phi}(\bar{\lambda}, \bar{\lambda}, \bar{\theta}_1, \bar{\theta}_2), \qquad \widehat{\Phi}^{PS}(\bar{\lambda}, \bar{\theta}_1, \bar{\theta}_2) = \widehat{\Phi}(\bar{\lambda}, 1, \bar{\theta}_1, \bar{\theta}_2), \tag{53}$$

corresponding to general *non-aligned* axisymmetric and pure shear loadings, respectively (cf., (29)). Similarly, we introduce the notations

$$\widehat{\phi}^{AS}(\bar{\lambda}, \bar{\theta}) = \widehat{\phi}(\bar{\lambda}, \bar{\lambda}, \bar{\theta}), \qquad \widehat{\phi}^{PS}(\bar{\lambda}, \bar{\theta}) = \widehat{\phi}(\bar{\lambda}, 1, \bar{\theta}), \tag{54}$$

respectively for axisymmetric and pure shear loadings with $\theta_1 = 0$ (cf., (30)).

5.1. *Axisymmetric Shear*

Here, we begin by considering the SE condition for *non-aligned* axisymmetric loadings, characterized by $\bar{\lambda}_1 = \bar{\lambda}_2 = \bar{\lambda}$ in the loading form (24). For this case, the numerical results show that the critical unit vectors at which the inequality (47) cease to hold, take the form $\mathbf{m}_{cr} = \mathbf{e}_2$ and $\mathbf{n}_{cr} = \cos(\alpha_{cr})\mathbf{e}_1 + \sin(\alpha_{cr})\mathbf{e}_3$. In view of these results for the critical vectors $\mathbf{m}_{cr}$ and $\mathbf{n}_{cr}$, it is inferred that the macroscopic instability, under non-aligned loading condition, consistently takes places through development of *localized* shear deformations (also known as "*shear bands*") on all planes whose normal lies in the $\mathbf{e}_1 - \mathbf{e}_3$ plane, and in the $\mathbf{e}_2$ direction. In this connection, α_{cr} serves to characterize the angle between the normal to the plane of the "shear band" and the $\mathbf{e}_1$ direction, *exactly* at the moment of shear band initiation. The corresponding normal vector in the undeformed configuration can be obtained from relation $\mathbf{N}_{cr} = \bar{\mathbf{F}}_{cr}^T \mathbf{n}_{cr}$. Using the resulting vectors $\mathbf{n}_{cr}$, and $\mathbf{m}_{cr}$ in condition (47), it can be deduced that macroscopic instabilities may first develop along *non-aligned* axisymmetric shear loading paths whenever the quadratic equation

$$\widehat{L}^c_{2121}\left(\frac{n_1}{n_3}\right)^2 + 2\widehat{L}^c_{2321}\left(\frac{n_1}{n_3}\right) + \widehat{L}^c_{2323} = 0 \tag{55}$$

admits real roots for n_1/n_3. Consequently, necessary and sufficient condition for the quadratic equation to have complex roots can be expressed as

$$\widehat{L}^c_{2121}\widehat{L}^c_{2323} - \left(\widehat{L}^c_{2321}\right)^2 > 0. \tag{56}$$

Making use of the expressions for the L^c_{2121}, L^c_{2323}, and L^c_{2321}, provided in Appendix D, for axisymmetric shear loading, the associated SE condition for the effective stored-energy

function $\widehat{\Phi}$ can be written as

$$\Big\{\Big[\bar{\lambda}\sin^2(\bar{\theta})\widehat{\Phi}_{,\bar{\lambda}_1\bar{\lambda}_1\bar{\theta}_1\bar{\theta}_1}-\bar{\lambda}\sin(\bar{\theta})\cos(\bar{\theta})\,\widehat{\Phi}_{,\bar{\lambda}_1\bar{\lambda}_1\bar{\theta}_2}+6\,\widehat{\Phi}_{,\bar{\lambda}_1\bar{\lambda}_1}\,\bar{\lambda}+2\,\bar{\lambda}\,\widehat{\Phi}_{,\bar{\lambda}_2\bar{\lambda}_2}+8\,\widehat{\Phi}_{,\bar{\lambda}_1}$$
$$-2\,\bar{\lambda}\,\widehat{\Phi}^{AS}_{,\bar{\lambda}\bar{\lambda}}-2\,\widehat{\Phi}^{AS}_{,\bar{\lambda}}\Big]\times\Big[\bar{\lambda}^5\sin(\bar{\theta})\cos(\bar{\theta})\widehat{\Phi}_{,\bar{\theta}_2}+\bar{\lambda}^5\cos^2(\bar{\theta})\,\widehat{\Phi}_{,\bar{\theta}_1\bar{\theta}_1}+(\bar{\lambda}^6-1)\widehat{\Phi}_{,\bar{\lambda}_2}\Big]$$
$$-2\,\bar{\lambda}^2\,(\bar{\lambda}^6-1)^{-2}\Big\{2\,\bar{\lambda}\,(2\,\bar{\lambda}^6\cos^2(\bar{\theta})-1)\,\widehat{\Phi}_{,\bar{\theta}_2}+\bar{\lambda}^2\,(\bar{\lambda}^6-1)\cos^2(\bar{\theta})\,\widehat{\Phi}_{,\bar{\lambda}_1\bar{\theta}_2}$$
$$-\bar{\lambda}^2\sin(\bar{\theta})\cos(\bar{\theta})\Big[4\,\bar{\lambda}^5\,\widehat{\Phi}_{,\bar{\theta}_1\bar{\theta}_1}+(\bar{\lambda}^6-1)\widehat{\Phi}_{,\bar{\lambda}_1\bar{\theta}_1\bar{\theta}_1}\Big]\Big\}^2\Big\}\Big|_{\substack{\bar{\lambda}_1=\bar{\lambda}_2=\bar{\lambda},\\ \bar{\theta}_1=0,\,\bar{\theta}_2=\bar{\theta}}}>0. \tag{57}$$

Recall that the above condition is calculated at $\bar{\theta}_1=0^\circ$, and the axisymmetric shear conditions $\bar{\lambda}_1=\bar{\lambda}_2=\bar{\lambda}$ should be applied to all terms after taking derivatives. Loss of ellipticity is therefore expected at the critical stretch $\bar{\lambda}_{cr}$ for which condition (57) is first violated. The corresponding critical angle α_{cr} can be shown to be given by

$$\alpha_{cr}=\bar{\theta}+\tan^{-1}\Big\{\bar{\lambda}\,\Big\{2\,\bar{\lambda}\,(2\,\bar{\lambda}^6\cos^2(\bar{\theta})-1)\widehat{\Phi}_{,\bar{\theta}_2}+\bar{\lambda}^2(\bar{\lambda}^6-1)\cos^2(\bar{\theta})\widehat{\Phi}_{,\bar{\lambda}_1\bar{\theta}_2}$$
$$-\bar{\lambda}^2\sin(\bar{\theta})\cos(\bar{\theta})\Big[4\,\bar{\lambda}^5\,\widehat{\Phi}_{,\bar{\theta}_1\bar{\theta}_1}+(\bar{\lambda}^6-1)\widehat{\Phi}_{,\bar{\lambda}_1\bar{\theta}_1\bar{\theta}_1}\Big]\Big\}$$
$$\times\frac{1}{2}\Big[\bar{\lambda}^5\cos(\bar{\theta})\sin(\bar{\theta})\widehat{\Phi}_{,\bar{\theta}_2}+\bar{\lambda}^5\widehat{\Phi}_{,\bar{\theta}_1\bar{\theta}_1}\cos^2(\bar{\theta})+(\bar{\lambda}^6-1)\widehat{\Phi}_{,\bar{\lambda}_2}\Big]^{-1}\Big\}\Big|_{\substack{\bar{\lambda}_1=\bar{\lambda}_2=\bar{\lambda}_{cr},\\ \bar{\theta}_1=0,\,\bar{\theta}_2=\bar{\theta}}}. \tag{58}$$

Note that the above expression is calculated at $\bar{\lambda}_{cr}$.

Next, we consider the development of macroscopic instabilities for the composites subjected to the *aligned* axisymmetric loading of the form (38). In this case, the result depends on whether the particles are *prolate* ($w>1$), or *oblate* ($w<1$), and these two cases are considered separately below.

Prolate particles. Here, we consider composites consisting of an incompressible matrix and aligned prolate spheroidal particles (see Fig. 1a) subjected to axisymmetric shear loading (38). In this case, within the context of condition (50), and based on the numerical examination, the loss of strong ellipticity for the effective stored-energy function $\widehat{\Phi}$ takes place when the vector $\mathbf{n}_{cr}$ is aligned with the $\mathbf{e}_3$ axis and the vector $\mathbf{m}_{cr}$ lies in the $\mathbf{e}_1-\mathbf{e}_2$ plane in the deformed configuration. That is, the homogenized composite material may develop localized shear deformations on the plane determined by the normal $\mathbf{e}_3$, and in all directions in the transverse plane. Using these vectors in the condition (50), it can be deduced that macroscopic instabilities may first develop along axisymmetric shear loading paths whenever the following inequality is first violated

$$\widehat{L}^c_{1313}=\widehat{L}^c_{2323}>0. \tag{59}$$

It should be noted that, for the case of prolate particles, the associated numerical results (to be discussed in more detail in Part II of this work) show that this type of instability occurs only when $\bar{\lambda}>1$. This regime of $\bar{\lambda}$ corresponds to the *equibiaxial tension* loading in the $\mathbf{e}_1-\mathbf{e}_2$ plane with the stretch $\bar{\lambda}$, which is equivalent to the *uniaxial compression* loading in the $\mathbf{e}_3$ direction with (compressive) stretch $1/\bar{\lambda}^2$. In other words, as the (compressive) stretching along the long axes of the particle increases, the effective incremental modu-

lus in the transverse plane perpendicular to the particle symmetry axes ($\widehat{L}^c_{1313} = \widehat{L}^c_{2323}$) *softens* to the point that it vanishes ($\widehat{L}^c_{1313} = 0$). This point is characterized by some finite critical stretch $\bar{\lambda}_{cr} > 1$. This localized behavior can be related to the evolution of the microstructure in the particle-reinforced elastomers. Thus, as will be seen in Part II, the loss of strong ellipticity would correspond to an abrupt rotation (or *flopping*) of the particles under a sufficiently large compressive loading. Making use of the expression for L^c_{1313} given in Appendix D, the associated strong ellipticity condition in terms of the effective stored-energy function can be given as

$$\left[\bar{\lambda}^5 \frac{\partial^2 \widehat{\phi}^{AS}}{\partial \bar{\theta}^2} + \frac{1}{2}(\bar{\lambda}^6 - 1)\frac{\partial \widehat{\phi}^{AS}}{\partial \bar{\lambda}}\right]\Bigg|_{\bar{\theta}=0^\circ} > 0. \tag{60}$$

Note that all derivatives in the above conditions are taken at $\bar{\theta} = 0^\circ$.

Oblate particles. Here, we consider composites consisting of an incompressible matrix and aligned oblate spheroidal particles (see Fig. 1(b)). In this case, along the loading path (38), the numerical study indicates that the strong ellipticity condition (50) is first violated when the vector $\mathbf{n}_{cr}$ lies in the $\mathbf{e}_1 - \mathbf{e}_2$ plane and the vector $\mathbf{m}_{cr}$ is aligned with the $\mathbf{e}_3$ direction in the deformed configuration. In other words, the homogenized composite material may develop localized shear deformations on all planes whose normal lies in the $\mathbf{e}_1 - \mathbf{e}_2$ plane, and in the $\mathbf{e}_3$ direction. Using these vectors in the condition (50), it is easy to show that the first macroscopic instabilities may develop along axisymmetric shear loading paths whenever the following inequality is first violated

$$\widehat{L}^c_{3131} = \widehat{L}^c_{3232} > 0. \tag{61}$$

It is remarked that, for the case of oblate particles, the numerical results show that this instability occurs only for $0 < \bar{\lambda} < 1$. This regime of $\bar{\lambda}$ corresponds to a *equibiaxial compression* loading in the $\mathbf{e}_1 - \mathbf{e}_2$ plane with (compressive) stretch $\bar{\lambda}$, which is equivalent to the *uniaxial tension* loading in the $\mathbf{e}_3$ direction with (tensile) stretch $1/\bar{\lambda}^2$. That is, as the (compressive) stretching in the transverse plane increases, the effective incremental modulus in all planes with the normal vector $\mathbf{n} \in \mathrm{Span}\{\mathbf{e}_1 - \mathbf{e}_2\}$ *softens* to the point that it vanishes ($\widehat{L}^c_{3131} = \widehat{L}^c_{3232} = 0$). Making contact with the microstructure, the loss of strong ellipticity can be identified with flopping of the oblate particles under compressive loading in the $\mathbf{e}_1 - \mathbf{e}_2$ plane. Making use of the expression for $\widehat{L}^c_{3131}$, given in Appendix D, the associated strong ellipticity condition in terms of the effective stored-energy function can be written as

$$\left[2\frac{\partial^2 \widehat{\phi}^{AS}}{\partial \bar{\theta}^2} + \bar{\lambda}(\bar{\lambda}^6 - 1)\frac{\partial \widehat{\phi}^{AS}}{\partial \bar{\lambda}}\right]\Bigg|_{\bar{\theta}=0^\circ} > 0. \tag{62}$$

5.2. *Pure shear*

In this subsection, we consider the case of particle-reinforced elastomers subjected to pure shear deformations, characterize by $\bar{\lambda}_1 = \bar{\lambda}, \bar{\lambda}_2 = 1$ in expression (24). In this case, similar to the case of non-aligned axisymmetric shear loading, the strong ellipticity condition (47) is violated at the critical vectors $\mathbf{m}_{cr} = \mathbf{e}_2$ and $\mathbf{n}_{cr} = \cos(\alpha_{cr})\mathbf{e}_1 + \sin(\alpha_{cr})\mathbf{e}_3$. In turn, the same strong ellipticity condition (56) is obtained for the case of non-aligned pure shear loading. Making use of the expressions for the L^c_{2121}, L^c_{2323}, and L^c_{2321} given in Appendix D for pure shear loading, the following macroscopic onset-of-failure surface $(\bar{\lambda}, \bar{\theta})$ is

obtained

$$\Big\{\Big[\cos(\bar\theta)\sin(\bar\theta)\widehat\Phi_{,\bar\theta_2}-\sin^2(\bar\theta)\widehat\Phi_{,\bar\theta_1\bar\theta_1}-\left(\bar\lambda^2-1\right)\left(\bar\lambda\,\widehat\Phi_{,\bar\lambda_1}-\widehat\Phi_{,\bar\lambda_2}\right)\Big]\bar\lambda^2$$
$$\times\Big[\left(\bar\lambda^2-1\right)\widehat\Phi_{,\bar\lambda_2}+\bar\lambda^2\sin(\bar\theta)\cos(\bar\theta)\widehat\Phi_{,\bar\theta_2}+\bar\lambda^2\cos^2(\bar\theta)\,\widehat\Phi_{,\bar\theta_1\bar\theta_1}\Big]-\bar\lambda^4\left(\bar\lambda^2+1\right)^{-2}$$
$$\times\Big[\left(\bar\lambda^2\cos^2(\bar\theta)-\sin^2(\bar\theta)\right)\widehat\Phi_{,\bar\theta_2}-\left(\bar\lambda^2+1\right)\sin(\bar\theta)\cos(\bar\theta)\widehat\Phi_{,\bar\theta_1\bar\theta_1}\Big]^2\Big\}\Big|_{\substack{\bar\lambda_1=\bar\lambda,\,\bar\lambda_2=1,\\ \bar\theta_1=0,\,\bar\theta_2=\bar\theta}}>0. \quad (63)$$

Note that the SE condition (63) is calculated at $\bar\theta_1=0^\circ$, and the pure shear conditions $\bar\lambda_1=\bar\lambda$, $\bar\lambda_2=1$ should be applied to all terms after taking derivatives. Also, for the cases in which the strong ellipticity condition (63) is violated, the corresponding critical angle α_{cr}, characterizing the angle between the $\mathbf{e}_1$ axis and the normal to the shear band plane at the moment of its initiation, can be shown to be obtained by

$$\alpha_{cr}=\bar\theta+\tan^{-1}\Big\{\bar\lambda^2\Big[\left(\bar\lambda^2\cos^2(\bar\theta)-\sin^2(\bar\theta)\right)\widehat\Phi_{,\bar\theta_2}-\sin(\bar\theta)\cos(\bar\theta)\left(\bar\lambda^2+1\right)\widehat\Phi_{,\bar\theta_1\bar\theta_1}\Big]$$
$$\times\Big\{\left(\bar\lambda^2+1\right)\Big[\left(\bar\lambda^2-1\right)\widehat\Phi_{,\bar\lambda_2}+\bar\lambda^2\sin(\bar\theta)\cos(\bar\theta)\widehat\Phi_{,\bar\theta_2}+\bar\lambda^2\cos^2(\bar\theta)\,\widehat\Phi_{,\bar\theta_1\bar\theta_1}\Big]\Big\}^{-1}\Big\}\Big|_{\substack{\bar\lambda_1=\bar\lambda_{cr},\,\bar\lambda_2=1,\\ \bar\theta_1=0,\,\bar\theta_2=\bar\theta}}. \quad (64)$$

Recall that the above expression is calculated at $\bar\lambda_{cr}$, corresponding to the stretch at which the shear band is initiated.

Next, we consider the development of macroscopic instabilities for the composites subjected to the aligned pure shear loading of the form (41). Similar to the case of axisymmetric loadings, the two classes of microstructures with *prolate* and *oblate* particles (see Fig. 1a, b) should be examined separately.

Prolate particles. For the case of prolate particles (see Fig. 1a), the strong ellipticity condition (50) is violated at the critical vectors $\mathbf{n}_{cr}=\mathbf{e}_3$ and $\mathbf{m}_{cr}\in\mathrm{Span}\{\mathbf{e}_1-\mathbf{e}_2\}$. Making use of these vectors in condition (50), it is concluded that the particle-reinforced materials become unstable under the aligned pure shear loading whenever any of the following inequalities is violated

$$\widehat L^c_{1313}>0,\quad \widehat L^c_{2323}>0. \quad (65)$$

In fact, the "failure mechanism" for both aligned pure shear and axisymmetric shear loadings is essentially the same, which is the softening of the effective incremental shear response perpendicular to the $\mathbf{e}_3$ direction. However, at the point of instability in the pure shear case, the overall shear response of the composite in the transverse plane vanishes in a *particular* direction within this plane ($\mathbf{e}_1$ or $\mathbf{e}_2$), while in the axisymmetric shear case, as mentioned earlier, it vanishes in *all* directions within the transverse plane. Making contact with evolution of the microstructure, this implies that, under aligned pure shear loading, the prolate particles "flop" about either the $\mathbf{e}_1$ or $\mathbf{e}_2$ directions depending on the other microstructural variables (w and c), while, under aligned axisymmetric shear loading, the flopping of the particles about any axis $\mathbf{m}\in\mathrm{Span}\{\mathbf{e}_1-\mathbf{e}_2\}$ is essentially the same. Now, making use of the pertinent expressions in Appendix D for aligned pure shear loading, the necessary and sufficient conditions for the associated effective stored-energy function $\widehat\Phi$

to be strongly elliptic can be expressed as

$$\left\{\bar{\lambda}\frac{\partial^2\widehat{\phi}^{PS^*}}{\partial\bar{\theta}^2}+(\bar{\lambda}^2-1)\left[\frac{\partial\widehat{\phi}^{PS}}{\partial\bar{\lambda}}-\left(\frac{\partial\widehat{\phi}}{\partial\bar{\lambda}_1}\right)\Big|_{\bar{\lambda}_1=\bar{\lambda},\bar{\lambda}_2=1}\right]\right\}\Big|_{\bar{\theta}=0^\circ}>0,$$
$$\left[\bar{\lambda}^3\frac{\partial^2\widehat{\phi}^{PS}}{\partial\bar{\theta}^2}+(\bar{\lambda}^4-1)\frac{\partial\widehat{\phi}^{PS}}{\partial\bar{\lambda}}\right]\Big|_{\bar{\theta}=0^\circ}>0, \tag{66}$$

where $\widehat{\phi}^{PS^*}(\bar{\lambda},\bar{\theta})=\widehat{\phi}(1,\bar{\lambda},\bar{\theta})$. (In the context of this last expression, it should be recalled that $\widehat{\Phi}(\bar{\lambda}_1,\bar{\lambda}_2,\bar{\theta},0)=\widehat{\Phi}(\bar{\lambda}_2,\bar{\lambda}_1,0,\bar{\theta})$.) Also, note that all derivatives in the above conditions are taken at $\bar{\theta}=0^\circ$, and the pure shear conditions $\bar{\lambda}_1=\bar{\lambda}$, $\bar{\lambda}_2=1$ should be applied to the term $\partial\widehat{\phi}/\partial\bar{\lambda}_1$.

Oblate particles. For the case of oblate particles (see Fig. 1b), the strong ellipticity condition (50) is violated at the critical vectors $\mathbf{n}_{cr}=\mathbf{e}_1$ and $\mathbf{m}_{cr}=\mathbf{e}_3$. Making use of these vectors in condition (50), it is deduced that the particle-reinforced materials first become unstable under aligned pure shear loading whenever the following inequality is violated

$$\widehat{L}^c_{3131}>0. \tag{67}$$

In this case, similar to the prolate particles case, the "failure mechanism" for both aligned pure shear and axisymmetric shear loadings is essentially the same, which is the softening of the effective incremental shear response along the $\mathbf{e}_3$ direction. The only difference is that, at the point of instability in the pure shear case, the overall shear response in the plane with normal vector $\mathbf{e}_1$ vanishes ($\widehat{L}^c_{3131}=0$); however, in the axisymmetric shear case, the overall shear response of the composite in *all* planes with the normal vector in the $\mathbf{n}\in\mathrm{Span}\{\mathbf{e}_1-\mathbf{e}_2\}$ vanishes ($\widehat{L}^c_{3131}=\widehat{L}^c_{3232}=0$). Now, making use of the pertinent expressions in Appendix D for aligned pure shear loading, the necessary and sufficient conditions for the associated effective stored-energy function $\widehat{\Phi}$ to be strongly elliptic can be expressed as

$$\left[\frac{\partial^2\widehat{\phi}^{PS}}{\partial\bar{\theta}^2}+\bar{\lambda}(\bar{\lambda}^4-1)\frac{\partial\widehat{\phi}^{PS}}{\partial\bar{\lambda}}\right]\Big|_{\bar{\theta}=0^\circ}>0. \tag{68}$$

Finally, note that for particular case of $w=1$, corresponding to spherical shape of particles, no loss of strong ellipticity is detected within the context of the condition (50). This observation, which is consistent with the results of Avazmohammadi and Ponte Castañeda [4] and Lopez-Pamies et al. [21], implies that the effective stored-energy function (35) is *strongly elliptic* in the limiting case of *spherical* particles. The results for general spheroidal particle shapes will be discussed in more detail in Part II of this paper.

6. Concluding Remarks

In this paper, we have made use of the tangent second-order, finite-strain homogenization framework proposed by Avazmohammadi and Ponte Castañeda [4] to estimate the overall response and microstructure evolution in incompressible elastomers reinforced by aligned, spheroidal, rigid particles, subject to general loading conditions. In particular, for *non-aligned* loadings, the analytical estimates (31) and (33) were derived for the effective stored-energy function of the composite and the rotation of the particles, respectively. For the special case of *aligned* loadings, explicit closed-form expressions were provided for

the effective stored-energy function of particle-reinforced neo-Hookean elastomers subjected to *axisymmetric* and *pure shear* loadings, as given in (39) and (42), respectively. It should be emphasized that the analytical results developed in this work are given in a form that can be easily implemented numerically into user-defined constitutive subroutines for use with standard finite element codes.

In this work, we also have presented a detailed study of the possible development of macroscopic instabilities in the particle-reinforced composites of interest, under both aligned and non-aligned loading conditions. The onset of such instabilities in these materials is identified with the loss of strong ellipticity of the associated homogenized behavior. In this connection, general conditions for loss of ellipticity were given in (49) and (51) for non-aligned and aligned loadings, respectively. These conditions were then specialized for the class of particulate composites undergoing axisymmetric and pure shear loadings in Subsections 5.1 and 5.2.

It should be remarked that, to the best of our knowledge, the estimates provided in this work for the effective stored-energy function and the particle rotation are the first homogenization-type estimates for reinforced elastomers with general spheroidal particle shape. The results are valid for large strains provided that the interfaces between the particles and the rubber remain intact. The estimates generalize the results of Avazmohammadi and Ponte Castañeda [4] for spherical particles, and are consistent with earlier results for continuous-fiber-reinforced elastomers [2, 3], as well as with simple laminates [10, 26], in the limits when the aspect ratio of the spheroidal particles tends to infinity and zero, respectively. It should also be noted that the results of this paper for the mechanical response of short-fiber-reinforced composites could be used to derive corresponding results for the magneto-elastic response of such composite materials when the particles are allowed to be magnetically susceptible (e.g., iron, nickel alloys) by means of the "partial decoupling approximation" introduced recently by Ponte Castañeda and Galipeau [33] (see also [34] for electro-active polymer composites).

In Part II of this paper, the analytical results provided in this part for the effective stored-energy function, rotation of particles, and development of the macroscopic instabilities will be explored in more detail for particle reinforced composites with neo-Hookean and Gent matrix phases. Explicit results will be presented for axisymmetric and pure shear loadings, as well as for a wide range of particles shapes and concentrations. Where possible, comparisons with full-field numerical simulations will be carried out.

Acknowledgements

This material is based upon work supported by the National Science Foundation under Grant No. CMMI-0969570. Parts of this article were written while PPC was visiting IMDEA Materials Institute in Madrid, Spain.

Appendix A. Calculation of the tensor E

In this appendix, we recall from our earlier paper [4] the procedure for calculating the tensor $\mathbf{E}$ for a given stored-energy function $W_\mu^{(1)}$, macroscopic deformation gradient $\bar{\mathbf{F}}$, and shape tensor $\mathbf{Z}_0$. Thus,

$$\mathbf{E} = \mathbf{Q}_0 - \mathbf{L}_\mu^{(1)}, \tag{A1}$$

where

$$\mathbf{Q}_0 = \mathbf{P}_0^{\dagger}(\boldsymbol{\mathscr{I}} - \mathbf{P}_1\mathbf{Q}_{-1}) + \sum_{i=1}^{3} \mathbf{W}_i \otimes \mathbf{V}_i^{(1)}, \tag{A2}$$

with

$$\mathbf{Q}_{-1} = \sum_{i=1}^{3} \mathbf{W}_i \otimes \mathbf{V}_i^{(0)}. \tag{A3}$$

In the above equations, $\{\mathbf{W}_1, \mathbf{W}_2, \mathbf{W}_3\}$ is a set of second-order tensor spanning the null space of $\mathbf{P}_0$, while the second order tensors $\mathbf{V}_i^{(0)}$and $\mathbf{V}_i^{(1)}$ are defined by [5]

$$\mathbf{V}_i^{(0)} = \frac{1}{\mathbf{W}_i \cdot \mathbf{P}_1 \mathbf{W}_i} \mathbf{W}_i, \tag{A4}$$

and

$$\mathbf{V}_i^{(1)} = -\frac{1}{\mathbf{W}_i \cdot \mathbf{P}_1 \mathbf{W}_i} \left\{ (\mathbf{P}_1 \mathbf{P}_0^{\dagger})^T \mathbf{W}_i + \left[\mathbf{W}_i . (\mathbf{P}_2 - \mathbf{P}_1 \mathbf{P}_0^{\dagger} \mathbf{P}_1) \mathbf{W}_i \right] \mathbf{V}_i^{(0)} \right\}, \tag{A5}$$

where $i = 1,2,3$ (no sum), and where the superscript T denotes the usual transpose of a fourth-order tensor (i.e., $(\cdot)^T_{ijkl} = (\cdot)_{klij}$). In addition, $\mathbf{P}_0^{\dagger}$ is the Moore-Penrose generalized inverse of $\mathbf{P}_0$ satisfying the properties

$$\begin{aligned} &\mathbf{P}_0 \mathbf{P}_0^{\dagger} \mathbf{P}_0 = \mathbf{P}_0, \qquad \mathbf{P}_0^{\dagger} \mathbf{P}_0 \mathbf{P}_0^{\dagger} = \mathbf{P}_0^{\dagger}, \\ &(\mathbf{P}_0 \mathbf{P}_0^{\dagger})^T = \mathbf{P}_0 \mathbf{P}_0^{\dagger}, \qquad (\mathbf{P}_0^{\dagger} \mathbf{P}_0)^T = \mathbf{P}_0^{\dagger} \mathbf{P}_0, \end{aligned} \tag{A6}$$

where the tensors $\mathbf{P}_0$, $\mathbf{P}_1$, and $\mathbf{P}_2$ are given by

$$(P_r)_{ijkl} = \frac{1}{4\pi |\mathbf{Z}_0|} \int_{|\boldsymbol{\xi}|=1} (B_r)_{ik} \xi_j \xi_l \left[\boldsymbol{\xi}^T (\mathbf{Z}_0^T \mathbf{Z}_0)^{-1} \boldsymbol{\xi} \right]^{-\frac{3}{2}} dS, \quad r = 0,1,2. \tag{A7}$$

Note that the tensor $\mathbf{P}_0$ is the limiting value of the tensor $\mathbf{P}$ (defined in (18)) in the incompressible matrix limit. The second-order tensors $\mathbf{B}_r$, $r = 1,2,3$ in (A7) can be obtained by

$$\begin{aligned} \mathbf{B}_0 &= \frac{1}{d_0} \mathbf{D}_0, \\ \mathbf{B}_1 &= \frac{1}{d_0} \left(\mathbf{D}_1 - \frac{d_1}{d_0} \mathbf{D}_0 \right), \\ \mathbf{B}_2 &= \frac{d_1}{(d_0)^3} \left(d_1 \mathbf{D}_0 - d_0 \mathbf{D}_1 \right), \end{aligned} \tag{A8}$$

where d_0 and d_1 are given by

$$\begin{aligned} d_0 &= \frac{1}{6} e_{ijk} e_{pqr} \left[(K_\mu)_{ip} (K_\mu)_{jq} (K_{-1})_{kr} + (K_\mu)_{ip} (K_{-1})_{jq} (K_\mu)_{kr} + (K_{-1})_{ip} (K_\mu)_{jq} (K_\mu)_{kr} \right], \\ d_1 &= \det(\mathbf{K}_\mu) = \frac{1}{6} e_{ijk} e_{pqr} (K_\mu)_{ip} (K_\mu)_{jq} (K_\mu)_{kr}, \end{aligned} \tag{A9}$$

and the tensors $\mathbf{D}_0$ and $\mathbf{D}_1$ have components

$$(D_0)_{ik} = e_{irs}e_{kpq}(K_\mu)_{rp}(K_{-1})_{sq},$$
$$(D_1)_{ik} = \frac{1}{2}e_{irs}e_{kpq}(K_\mu)_{rp}(K_\mu)_{sq}. \tag{A10}$$

Finally, the second-order tensors $\mathbf{K}_\mu$ and $\mathbf{K}_{-1}$ in (A9) and (A10) are the parts of the acoustic tensor $\mathbf{K}$ (defined in the context of (18)) associated with the "incompressible" and "compressible" parts of the moduli tensor $\mathbf{L}^{(1)}$. These two parts of the tensor $\mathbf{L}^{(1)}$, denoted by $\mathbf{L}^{(1)}_\mu$ and $\mathbf{L}^{(1)}_{-1}$, respectively, defined in (6). Hence, the tensors $\mathbf{K}_{-1}$ and $\mathbf{K}_\mu$ are determined by the following relations

$$(K_\mu)_{ik} = (L_\mu)^{(1)}_{ijkl}\,\xi_j\xi_l, \qquad (K_{-1})_{ik} = (L_{-1})^{(1)}_{ijkl}\,\xi_j\xi_l. \tag{A11}$$

In general, a Gaussian quadrature technique can be implemented for the numerical computations of the integrals (A7) over the surface of the unit sphere, $|\boldsymbol{\xi}| = 1$. However, it is noted that, for a given microstructure, and for certain types of matrix behaviors and loading conditions, these integrals can be calculated analytically, leading to closed-form expressions for the components of the tensor $\mathbf{E}$. This is the case for spheroidal particles in a neo-Hookean matrix subjected to aligned loadings. The relevant components of the tensors $\mathbf{P}_r$ for this case are given in Appendix C.

Appendix B. Calculation of the tensors $\mathbf{P}_r$ for spheroidal particles embedded in a generalized neo-Hookean matrix under non-aligned loadings

In this appendix, we briefly address the numerical calculation of the integrals (A7) for the case of spheroidal particles embedded in an incompressible matrix of the form (21) subjected to non-aligned loadings (24) (note that $\bar{\theta}_1 = 0^\circ$). For this purpose, we make use of polar cylindrical coordinates, and parametrize the unit vector $\boldsymbol{\xi}$ in (A7) as

$$\xi_1 = \sqrt{1-z^2}\cos(\theta), \quad \xi_2 = \sqrt{1-z^2}\sin(\theta), \quad \xi_3 = z, \tag{B1}$$

in which θ and z vary over the intervals $0 \le \theta \le \pi$ and $0 \le z \le 1$. Now, making use of (B1), and setting $\mathbf{Z}_0 = \mathrm{diag}(1,1,w)$ for the spherical particles, the integrals (A7) yield to the following double integrals

$$(P_r)_{ijkl} = \frac{w}{4\pi}\int_0^\pi \int_0^1 \frac{(B_r)_{ik}}{[1+(w^2-1)z^2]^{3/2}}\,\mathrm{d}\theta\,\mathrm{d}z, \quad r = 0,1,2. \tag{B2}$$

In order to compute the above integrals, it proves helpful to provide the corresponding analytical expression for the tensors $\mathbf{B}_r$, $r = 1,2,3$, which can be determined from those of the second-order tensors $\mathbf{D}_0$ and $\mathbf{D}_1$ as well as the scalars d_0 and d_1 by using relations (A8). For general non-aligned loadings (24) and general matrix behavior (21), the analytical expressions for $\mathbf{D}_0$, $\mathbf{D}_1$, d_0 and d_1 are too cumbersome to be included here, and instead, we present the expressions for the tensors $\mathbf{K}_\mu$ and $\mathbf{K}_{-1}$ from which the corresponding expressions for $\mathbf{D}_0$, $\mathbf{D}_1$, d_0 and d_1 can be easily obtained with the help of relations (A9) and (A10). In this case, the components of the symmetric, second-order tensors $\mathbf{K}_\mu$ and

$\mathbf{K}_{-1}$ read as

$$(K_\mu)_{11} = 2\,g_I + 4(V_1\,\xi_1 - V_3\,\xi_3)^2 g_{II} + (V_2\,\xi_1 + V_3\,\xi_3)^2\,\bar{\lambda}_2^2\,h_{JJ},\ \ (K_\mu)_{22} = 2\,g_I + (4\,\bar{\lambda}_2^2 g_{II} + h_{JJ}/\bar{\lambda}_2^2)\xi_2^2,$$
$$(K_\mu)_{33} = 2\,g_I + 2\,(V_3\,\xi_1 - V_2\,\xi_3)^2 g_{II} + (V_3\,\xi_1 + V_1\,\xi_3)^2\bar{\lambda}_2^2\,h_{JJ},$$
$$(K_\mu)_{12} = \left[4\,\bar{\lambda}_2(V_1\,\xi_1 - V_3\,\xi_3)g_{II} + (V_2\,\xi_1 + V_3\,\xi_3)\,h_{JJ}\right]\,\xi_2,$$
$$(K_\mu)_{23} = \left[4\,\bar{\lambda}_2(V_2\,\xi_3 - V_3\,\xi_1)g_{II} + (V_3\,\xi_1 + V_1\,\xi_3)\,h_{JJ}\right]\,\xi_2,$$
$$(K_\mu)_{13} = 4\left[(2V_3^2 + \bar{\lambda}_2^{-1})\xi_1\xi_3 - V_3(V_1\xi_1^2 + V_2\xi_3^2)\right]g_{II} + \bar{\lambda}_2^2\left[(2V_3^2 + \bar{\lambda}_2^{-1})\xi_1\xi_3 + V_3(V_1\xi_3^2 + V_2\xi_1^2)\right]h_{JJ},$$

and

$$(K_{-1})_{11} = (V_2\,\xi_1 + V_3\,\xi_3)^2\,\bar{\lambda}_2^2, \quad (K_{-1})_{22} = \xi_2^2/\bar{\lambda}_2^2, \quad (K_{-1})_{33} = (V_3\,\xi_1 + V_1\,\xi_3)^2\,\bar{\lambda}_2^2,$$
$$(K_{-1})_{12} = (V_2\,\xi_1 + V_3\,\xi_3)\xi_2, \quad (K_{-1})_{23} = (V_3\,\xi_1 + V_1\,\xi_3)\xi_2,$$
$$(K_{-1})_{13} = \left[(2V_3^2 + \bar{\lambda}_2^{-1})\xi_1\xi_3 + (V_2\xi_1^2 + V_1\xi_3^2)V_3\right]\bar{\lambda}_2^2, \tag{B3}$$

where

$$V_1 = \bar{\lambda}_1\cos(\bar{\theta})^2 + \left(\bar{\lambda}_1\bar{\lambda}_2\right)^{-1}\sin(\bar{\theta})^2, \quad V_2 = \bar{\lambda}_1\sin(\bar{\theta})^2 + \left(\bar{\lambda}_1\bar{\lambda}_2\right)^{-1}\cos(\bar{\theta})^2$$
$$V_3 = \left[\bar{\lambda}_1 - \left(\bar{\lambda}_1\bar{\lambda}_2\right)^{-1}\right]\sin(\bar{\theta})\cos(\bar{\theta}).$$

For the special case of neo-Hookean matrix given by (23), the final expressions for d_0, d_1 and $\mathbf{D}_0$, $\mathbf{D}_1$ can be simplified considerably. In this case, the expressions for d_0 and d_1 are given by

$$d_0 = (\mu^{(1)})^2(u_2\xi_1^2 + u_3\xi_1\xi_3 + u_1\xi_3^2 + t^2\,\bar{\lambda}_1^4\,\xi_2^2)\bar{\lambda}_2^2, \qquad d_1 = \mu^{(1)}d_0 + (\mu^{(1)})^3. \tag{B4}$$

Also, the corresponding components of the symmetric matrices $\mathbf{D}_0$ and $\mathbf{D}_1$ read as

$$(D_0)_{11} = \mu^{(1)}\,\bar{\lambda}_2^2\left(V_3^2\xi_1^2 + t^2\,\bar{\lambda}_1^4\,\xi_2^2 + V_1^2\xi_3^2 + 2V_1V_3\,\xi_1\xi_3\right), \qquad (D_0)_{22} = \mu^{(1)}\,\bar{\lambda}_2^2(u_2\xi_1^2 + u_3\xi_1\xi_3 + u_1\xi_3^2),$$
$$(D_0)_{33} = \mu^{(1)}\,\bar{\lambda}_2^2\left(V_2^2\xi_1^2 + t^2\,\bar{\lambda}_1^4\,\xi_2^2 + V_3^2\xi_3^2 + 2V_2V_3\,\xi_1\xi_3\right),$$
$$(D_0)_{12} = -\mu^{(1)}\,\xi_2(V_2\xi_1 + V_3\,\xi_3), \qquad (D_0)_{23} = -\mu^{(1)}\,\xi_2(V_3\xi_1 + V_1\,\xi_3),$$
$$(D_0)_{13} = -\mu^{(1)}\,\bar{\lambda}_2^2\left[V_2V_3\,\xi_1^2 + (2V_3^2 + \bar{\lambda}_2^{-1})\xi_1\xi_3 + V_1V_3\xi_3^2\right],$$

and

$$(D_1)_{11} = \mu^{(1)}(D_0)_{11} + (\mu^{(1)})^2, \quad (D_1)_{22} = \mu^{(1)}(D_0)_{22} + (\mu^{(1)})^2, \quad (D_1)_{33} = \mu^{(1)}(D_0)_{33} + (\mu^{(1)})^2,$$
$$(D_1)_{12} = \mu^{(1)}(D_0)_{12}, \quad (D_1)_{13} = \mu^{(1)}(D_0)_{13}, \quad (D_1)_{23} = \mu^{(1)}(D_0)_{23}, \tag{B5}$$

where $t = \left(\bar{\lambda}_1\bar{\lambda}_2\right)^{-2}$, and

$$u_1 = \bar{\lambda}_1^2\cos^2(\bar{\theta}) + t\,\sin^2(\bar{\theta}), \quad u_2 = t\,\cos^2(\bar{\theta}) + \bar{\lambda}_1^2\,\sin^2(\bar{\theta}), \quad u_3 = (\bar{\lambda}_1^2 - t)\sin(2\bar{\theta}). \tag{B6}$$

Finally, it is noted that for the special case of aligned loadings (34) with matrix behavior given by (21), we can make use of the analytical expressions for the tensors $\mathbf{D}_0$ and $\mathbf{D}_1$

and the scalars d_0 and d_1 provided in [4] for the case of spherical particles embedded in a matrix of the form (21) under isochoric, triaxial loadings of the form (34). This is because the tensors $\mathbf{D}_0$ and $\mathbf{D}_1$ and the scalars d_0 and d_1 do not contain any information about the shape of particles and depend only on the matrix behavior and loading conditions. These expressions are available in Eq. (131) and (132) in [4] and are not included here, for brevity.

In general, a Gaussian quadrature technique with a rather high numbers of Gauss points is needed for the numerical integrations of (B2). However, for the special case of a neo-Hookean matrix subjected to aligned loadings, the integrals (B2) can be evaluated analytically, and will be given in Appendix C.

Appendix C. Normal components of the tensor $\mathbf{P}_r, r = 1,2,3$ for spheroidal particles embedded in a neo-Hookean matrix under general aligned loading

In this appendix, we present explicit expressions for the normal components of the tensor $\mathbf{P}_r, r = 1,2,3$, associated with a spheroidal particle embedded in a neo-Hookean material subjected to the isochoric, aligned deformation of the form (34). It is recalled that these analytical expressions for the components of the tensors $\mathbf{P}_r$, defined by (A7), are needed to find the corresponding analytical expressions for the $\mathbf{E}$-tensor, using Eqs. (A1)-(A6). In turn, a corresponding analytical expression for the effective stored-energy function (35) is obtained by substituting the $\mathbf{E}$-tensor components. Making use of the neo-Hookean model (23) into equations (A8)-(A11), it follows that the normal components of $\mathbf{P}_r$, $r = 1,2,3$, after some algebra, can be expressed as

$$
\begin{aligned}
(P_0)_{1111} &= \bar{\lambda}_1^2\,(2\,\mu^{(1)}\,l_3^2\,\omega_1^2\,\omega_2\,\omega_3^4)^{-1}\,\Big\{\omega_1^2\,\omega_2\,\omega_3\,\Big[w\,(2\,\bar{\lambda}_1^2\bar{\lambda}_2^6-l_4)\,A_1+\omega_3\,(w^2 l_4-2\,\bar{\lambda}_1^2\bar{\lambda}_2^6)\Big]\\
&\quad -2\,w\,\bar{\lambda}_1\bar{\lambda}_2\,\Big\{\omega_2^4\,\omega_3^2\,\Xi_{e1}-\omega_2^2\,\Big[w^2(\tfrac{1}{2}\mathrm{L}+1)+\bar{\lambda}_1^2\bar{\lambda}_2^2\,\mathrm{T}^{\bar{2},1}_{1,0}\Big]\,\Xi_{f1}+l_2^2\omega_1^2\,\Xi_{p3}\Big\}\Big\},\\
(P_0)_{2222} &= \bar{\lambda}_2^2\,(2\,\mu^{(1)}\,l_3^2\,\omega_2\,\omega_3^4)^{-1}\Big\{\omega_2\,\Big[w\,\omega_3\,(2\,\bar{\lambda}_1^6\bar{\lambda}_2^2-l_4)A_1+\omega_3^2\,(w^2 l_4-2\,\bar{\lambda}_1^6\bar{\lambda}_2^2)\Big]\\
&\quad -2\,w\bar{\lambda}_1\bar{\lambda}_2\,(\omega_1^2\omega_3^2\,\Xi_{e1}+l_1\,\omega_1^2\,\Xi_{f1}+l_1^2\,\Xi_{p3})\Big\},\\
(P_0)_{3333} &= (\mu^{(1)}\,\omega_1^2\,\omega_2\,\omega_3^5)^{-1}\,\big[\omega_1^2\omega_2\omega_3^2(wA_1-\omega_3)-w\,\bar{\lambda}_1^3\bar{\lambda}_2^3\,\omega_3^3\,\Xi_{e1}-w\,\bar{\lambda}_1^3\bar{\lambda}_2^3\,\omega_3\,\omega_1^2\,\Xi_{p3}\\
&\quad -w\,\bar{\lambda}_1^3\bar{\lambda}_2^3\,\omega_3\,\big(\bar{\lambda}_1^4\bar{\lambda}_2^2-2\,w^2+1\big)\,\Xi_{f1}\big],\\
(P_0)_{1122} &= -\bar{\lambda}_1\bar{\lambda}_2\,(2\,\mu^{(1)}\,l_3^2\,\omega_2\,\omega_3^4)^{-1}\,\big\{\omega_2\omega_3\,\big[w(2\,\bar{\lambda}_2^4\bar{\lambda}_1^4-l_4)\,A_1+\omega_3\,(w^2 l_4-2\,\bar{\lambda}_2^4\bar{\lambda}_1^4)\big]\\
&\quad -2\,w\,\bar{\lambda}_1\bar{\lambda}_2\,\big(\omega_2^2\omega_3^2\,\Xi_{e1}+l_2\,\omega_1^2\,\Xi_{f1}+l_1 l_2\,\Xi_{p3}\big)\big\},\\
(P_0)_{1133} &= \bar{\lambda}_1^2\bar{\lambda}_2^2\,(\mu^{(1)}\,l_3\,\omega_1^2\,\omega_2\,\omega_3^5)^{-1}\,\Big\{w\,\bar{\lambda}_1\,\omega_3\,\Big[(\bar{\lambda}_2^4\bar{\lambda}_1^2-\omega_2^2-1)w^2+\omega_2^2-\bar{\lambda}_1^6\bar{\lambda}_2^6+\bar{\lambda}_1^4\bar{\lambda}_2^2\Big]\,\Xi_{f1}\\
&\quad +w\,\omega_2^2\bar{\lambda}_1\,\omega_3^3\,\Xi_{e1}-w\,\bar{\lambda}_1\,\omega_3\,l_2\,\omega_1^2\,\Xi_{p3}+\bar{\lambda}_2\,\omega_1^2\,\omega_2\,\omega_3^2\,(wA_1-\omega_3)\big\},\\
(P_0)_{2233} &= -\bar{\lambda}_1^2\bar{\lambda}_2^2\,(\mu^{(1)}\,l_3\omega_2\,\omega_3^5)^{-1}\,\big[\bar{\lambda}_1\omega_2\omega_3^2(wA_1-\omega_3)+w\,\bar{\lambda}_2\omega_3\,\big(\omega_3^2\,\Xi_{e1}-\omega_1^2\,\Xi_{f1}-l_1\,\Xi_{p3}\big)\big],
\end{aligned}
$$

$$
\begin{aligned}
(P_1)_{1111} &= \bar{\lambda}_1^2\bar{\lambda}_2\,(2\,\mu^{(1)} l_3^2\,\omega_1^4\omega_2)^{-1}\left[w\bar{\lambda}_1\omega_2^2\left(w^2\,\mathrm{T}_{\bar{3}}^{1}+\bar{\lambda}_1^4\,\bar{\lambda}_2^2\,l_4\right)\Xi_{e1}-w\bar{\lambda}_1^3\bar{\lambda}_2^2 l_3\,\left(w^2\mathrm{T}_{\bar{3}}^{2}+\bar{\lambda}_1^4\,\bar{\lambda}_2^4\right)\Xi_{f1}\right.\\
&\quad\left.+\bar{\lambda}_2^3\,\omega_1^2\,\omega_2\left(2\,w^2-\bar{\lambda}_1^4\,l_4\right)\right],\\
(P_1)_{2222} &= \bar{\lambda}_1\bar{\lambda}_2^2(2\,\mu^{(1)}l_3^2\omega_2^3)^{-1}\left[w\bar{\lambda}_1^2\bar{\lambda}_2^5 l_3\,\Xi_{f1}-w\bar{\lambda}_2\left(w^2\,\mathrm{T}_{\bar{1}}^{3}-\bar{\lambda}_1^2\bar{\lambda}_2^4 l_4\right)\Xi_{e1}+\bar{\lambda}_1^3\omega_2(2\,w^2-\bar{\lambda}_2^4\,l_4)\right],\\
(P_1)_{3333} &= \bar{\lambda}_1\bar{\lambda}_2(2\,\mu^{(1)}\,\omega_1^3\omega_2^4)^{-1}\left[w(w^4+w^2\,\bar{\lambda}_1^2\bar{\lambda}_2^2\,l_4-3\bar{\lambda}_1^6\bar{\lambda}_2^6)\Xi_{e2}-w\bar{\lambda}_1^2\bar{\lambda}_2^2\left(w^2\mathrm{T}_{2}^{1}-3\,\bar{\lambda}_2^4\bar{\lambda}_1^4\right)\Xi_{f2}\right.\\
&\quad\left.-\bar{\lambda}_1^3\bar{\lambda}_2^3\,\omega_1\,\omega_2^2\right],\\
(P_1)_{1122} &= \bar{\lambda}_1^2\bar{\lambda}_2^2(2\,\mu^{(1)}l_3^2\omega_1^2\omega_2)^{-1}\left[w\left(w^2 l_4-2\,\bar{\lambda}_1^4\bar{\lambda}_2^4\right)\Xi_{e1}-w\bar{\lambda}_1^4\bar{\lambda}_2^2 l_3\,\Xi_{f1}-2\,\bar{\lambda}_1\bar{\lambda}_2\,\omega_2\,\omega_1^2\right],\\
(P_1)_{1133} &= \bar{\lambda}_1^3\bar{\lambda}_2^2(2\,\mu^{(1)}l_3\omega_1^4\omega_2)^{-1}\left[\bar{\lambda}_1\bar{\lambda}_2\,\omega_2\,\omega_1^2-w\left(w^2\mathrm{T}_{\bar{1}}^{2}-\bar{\lambda}_1^4\bar{\lambda}_2^4\right)\Xi_{e1}+w\,l_3\left(\bar{\lambda}_1^4\bar{\lambda}_2^2+w^2\right)\Xi_{f1}\right],\\
(P_1)_{2233} &= -\bar{\lambda}_1^2\bar{\lambda}_2^3(2\,\mu^{(1)}l_3\omega_1\omega_2^4)^{-1}\left[\bar{\lambda}_1\bar{\lambda}_2\omega_1\omega_2^2+w\left(w^2\mathrm{T}_{\bar{2}}^{1}+\bar{\lambda}_1^4\bar{\lambda}_2^4\right)\Xi_{e2}-w\,l_3\left(\bar{\lambda}_2^4\bar{\lambda}_1^2+w^2\right)\Xi_{f2}\right],
\end{aligned}
$$

$$
\begin{aligned}
(P_2)_{1111} &= -\bar{\lambda}_1^2\bar{\lambda}_2(8\,\mu^{(1)}l_3^2\omega_1^6\omega_2)^{-1}\left\{w\bar{\lambda}_1\left[\left(\mathrm{Y}_{3,0}^{3,\bar{6}}+\mathrm{T}_{\overline{12}}^{4}\right)w^6+\left(\mathrm{Y}_{\bar{3},12}^{\bar{7},12}+\mathrm{P}_{0,0}^{7,\bar{9}}+12\,\bar{\lambda}_1^2\bar{\lambda}_2^6\right)w^4\right.\right.\\
&\quad-w^2\,\bar{\lambda}_1^4\bar{\lambda}_2^2\left(\mathrm{Y}_{6,4}^{1,\bar{3}}+\mathrm{P}_{0,\bar{9}}^{2,3}+\mathrm{L}_{16}^{4}\right)+\bar{\lambda}_1^8\bar{\lambda}_2^6\left({}_{4}^{4}\mathrm{L}_0^2+\mathrm{T}_{1,\bar{4}}^{1,0}\right)\left.\right]\Xi_{e1}-w\bar{\lambda}_1 l_3\left[\left(\tfrac{8}{\overline{12}}\mathrm{L}_0^9+\mathrm{T}_{3,\bar{9}}^{\bar{3},0}\right)w^4\right.\\
&\quad-\bar{\lambda}_1^4\bar{\lambda}_2^2\left(\tfrac{8}{16}\mathrm{L}_0^1+\mathrm{T}_{\bar{6}}^{5}\right)w^2+\bar{\lambda}_1^8\bar{\lambda}_2^6\mathrm{R}_{\bar{1},0}^{\bar{4},1}\left.\right]\Xi_{f1}+\bar{\lambda}_2\omega_1^2\omega_2\left[8\,w^4\bar{\lambda}_2^2-\bar{\lambda}_1^2\left({}_{12}^{4}\mathrm{L}_0^6+\mathrm{T}_{5,\bar{8}}^{\bar{3},0}\right)w^2\right.\\
&\quad\left.\left.+\bar{\lambda}_1^6\bar{\lambda}_2^2\left({}_{4}^{4}\mathrm{L}_0^2+\mathrm{T}_{1,\bar{4}}^{1,0}\right)\right]\right\},\\
(P_2)_{2222} &= -\bar{\lambda}_1\bar{\lambda}_2^2(8\,\mu^{(1)}l_3^2\,\omega_1^2\omega_2^5)^{-1}\left\{\bar{\lambda}_1\omega_1^2\omega_2\left[8\,w^4\bar{\lambda}_1^2+\bar{\lambda}_2^2\left(\mathrm{T}_{3,8}^{\bar{5},0}+{}_{\bar{4}}^{\overline{12}}\mathrm{L}_{\bar{6}}^{0}\right)w^2+\bar{\lambda}_1^2\bar{\lambda}_2^6\left(\mathrm{T}_{1,\bar{4}}^{1,0}+{}_{4}^{4}\mathrm{L}_0^0\right)\right]\right.\\
&\quad+w\bar{\lambda}_2\left[\left(\mathrm{T}_{4}^{\overline{12}}+\mathrm{Y}_{3,0}^{3,\bar{6}}\right)w^6+\left(\mathrm{P}_{7,\bar{9}}^{0,0}+\mathrm{Y}_{\bar{7},12}^{\bar{3},12}+12\,\bar{\lambda}_1^6\bar{\lambda}_2^2\right)w^4+\bar{\lambda}_2^4\bar{\lambda}_1^2\left(\mathrm{P}_{\bar{2},\bar{3}}^{0,9}+\mathrm{Y}_{\bar{1},\bar{4}}^{\bar{6},3}+\mathrm{L}_{\bar{4}}^{\overline{16}}\right)w^2\right.\\
&\quad\left.+\bar{\lambda}_2^8\bar{\lambda}_1^6\left({}_{4}^{4}\mathrm{L}_0^2+\mathrm{T}_{1,\bar{4}}^{1,0}\right)\right]\Xi_{e1}-w\bar{\lambda}_2 l_3\left[\left({}_{\bar{4}}^{0}\mathrm{L}_{\bar{6}}^{3}+\mathrm{T}_{3,3}^{\bar{3},0}\right)w^4+\bar{\lambda}_1^2\bar{\lambda}_2^6\left({}_{2}^{3}\mathrm{L}-\mathrm{Y}_{0,0}^{\bar{4},\bar{4}}-6\,\bar{\lambda}_1^6+1\right)w^2\right.\\
&\quad\left.\left.-\bar{\lambda}_1^6\,\bar{\lambda}_2^8\,\mathrm{R}_{1,2}^{4,\bar{3}}\right]\Xi_{f1}\right\},\\
(P_2)_{3333} &= (8\,\mu^{(1)}\,\bar{\lambda}_1\bar{\lambda}_2\omega_1^5\omega_2^6)^{-1}\left\{\bar{\lambda}_1^3\bar{\lambda}_2^3\omega_1\omega_2^2\left[w^4\,\mathrm{R}_{\bar{1},4}^{4,4}-\bar{\lambda}_1^2\bar{\lambda}_2^2\left({}_{4}^{4}\mathrm{L}+\mathrm{T}_{3,8}^{3,0}\right)w^2+\bar{\lambda}_1^6\bar{\lambda}_2^6\mathrm{R}_{7}^{4}\right]\right.\\
&\quad-w\left[w^8\,\mathrm{R}_{2,1}^{4,1}+\bar{\lambda}_1^2\bar{\lambda}_2^2\left(\mathrm{T}_{\bar{7},3}^{\bar{7},0}+\mathrm{L}_{7}^{7}\right)w^6-\bar{\lambda}_1^4\bar{\lambda}_2^4\left(\mathrm{Y}_{3,16}^{3,\overline{13}}+\mathrm{P}_{0,20}^{0,20}+\mathrm{L}_{4}^{4}\right)w^4+\bar{\lambda}_1^8\bar{\lambda}_2^8\left(\mathrm{T}_{10,21}^{10,0}+{}_{16}^{16}\mathrm{L}\right)w^2\right.\\
&\quad\left.-3\,\bar{\lambda}_1^{12}\bar{\lambda}_2^{12}\mathrm{R}_{5}^{4}\right]\Xi_{e2}+w\bar{\lambda}_1^2\bar{\lambda}_2^2\left[\left(\mathrm{T}_{1,3}^{\bar{1},0}+{}_{8}^{4}\mathrm{L}_5^4\right)w^6-\bar{\lambda}_1^2\bar{\lambda}_2^2\left(\mathrm{Y}_{9,24}^{3,3}+\mathrm{P}_{\bar{3},13}^{0,11}+\mathrm{L}_{8}^{4}\right)w^4\right.\\
&\quad\left.\left.+2\,\bar{\lambda}_1^6\bar{\lambda}_2^6\left(\mathrm{T}_{10,6}^{5,0}+{}_{10}^{8}\mathrm{L}_{\bar{3}}^{0}\right)w^2+3\,\bar{\lambda}_1^{10}\bar{\lambda}_2^{10}\mathrm{R}_{\bar{5},1}^{\bar{4},0}\right]\Xi_{f2}\right\},\\
(P_2)_{1122} &= \bar{\lambda}_1^2\bar{\lambda}_2^2(8\,\mu^{(1)}l_3^2\omega_1^2\omega_2^4)^{-1}\left\{\bar{\lambda}_1\bar{\lambda}_2\omega_2^2\left[8\,w^4+\left({}_{\bar{8}}^{\bar{8}}\mathrm{L}_1^1-\mathrm{T}_{1}^{1}\right)w^2-\bar{\lambda}_1^4\bar{\lambda}_2^4\,\mathrm{R}_{\bar{2},1}^{\bar{8},1}\right]\omega_1\right.\\
&\quad-w\left[\left(\mathrm{Y}_{1,0}^{1,\bar{2}}+\mathrm{T}_{4}^{4}\right)w^6+\left(\mathrm{P}_{1,0}^{1,0}+\mathrm{Y}_{\bar{2},\overline{16}}^{\bar{2},2}-\mathrm{L}_{4}^{4}\right)w^4-2\,\bar{\lambda}_1^4\bar{\lambda}_2^4\left({}_{\bar{6}}^{\bar{6}}\mathrm{L}_1^1-l_4\right)w^2+\bar{\lambda}_1^8\bar{\lambda}_2^8\,\mathrm{R}_{\bar{2},1}^{\bar{8},1}\right]\Xi_{e2}\\
&\quad+w\,l_3\left[\left({}_{4}^{0}\mathrm{L}_{\bar{2}}^{1}+\mathrm{T}_{0,1}^{\bar{1},1}\right)w^4-\bar{\lambda}_2^6\bar{\lambda}_1^2\left(2\,\bar{\lambda}_1^6-4\,\bar{\lambda}_1^4-\mathrm{R}_{1,0}^{4,1}\right)w^2-\bar{\lambda}_2^8\bar{\lambda}_1^6\mathrm{R}_{1,0}^{4,\bar{1}}\right]\Xi_{f2}\left.\right\},
\end{aligned}
$$

$$
\begin{aligned}
(P_2)_{1133} &= -\bar{\lambda}_1 \left(8\,\mu^{(1)} l_3 \omega_1^6\, \omega_2^3\right)^{-1} \Big\{ \bar{\lambda}_1^3 \bar{\lambda}_2^3 \omega_1^2\, \omega_2 \left[\left(\mathrm{T}_{\bar{1}}^{3} + 4\right) w^4 + \left(\mathrm{T}_{1,\bar{2}}^{\bar{4},0} - {}_{4}^{4}\mathrm{L}_{0}^{\bar{1}}\right) w^2 + \bar{\lambda}_1^4 \bar{\lambda}_2^4\, \mathrm{R}_{3,0}^{4,\bar{1}}\right] \\
&\quad - w \left[\left({}_{\bar{4}}^{8}\mathrm{L}_{\bar{2}}^{7} + \mathrm{T}_{1,\bar{3}}^{\bar{1},0}\right) w^6 + \bar{\lambda}_1^2 \bar{\lambda}_2^2 \left(\mathrm{P}_{0,7}^{1,\overline{11}} + \mathrm{Y}_{1,\bar{8}}^{\bar{7},3} + \mathrm{L}_{4}^{\bar{8}}\right) w^4 - 2\,\bar{\lambda}_1^6 \bar{\lambda}_2^6 \left({}_{0}^{\bar{6}}\mathrm{L}_{0}^{1} - \mathrm{T}_{\bar{3},1}^{6,0}\right) w^2 - \bar{\lambda}_1^{10} \bar{\lambda}_2^{10} \mathrm{R}_{3,0}^{4,\bar{1}}\right] \Xi_{e1} \\
&\quad + w\, \bar{\lambda}_1^2 \bar{\lambda}_2^2\, l_3 \left[\left(\mathrm{T}_{1}^{3} + 4\right) w^6 + \left({}_{\bar{4}}^{0}\mathrm{L}_{0}^{5} - \mathrm{T}_{1,4}^{5,0}\right) w^4 - \bar{\lambda}_1^4 \bar{\lambda}_2^2 \left(4\,\bar{\lambda}_1^4 \bar{\lambda}_2^2 + \mathrm{T}_{\bar{6},5}^{3,0}\right) w^2 + \bar{\lambda}_1^8 \bar{\lambda}_2^6\, \mathrm{R}_{3,0}^{4,0}\right] \Xi_{f1} \Big\}, \\
(P_2)_{2233} &= -\bar{\lambda}_2 \left(8\,\mu^{(1)} l_3 \omega_1^4 \omega_2^5\right)^{-1} \Big\{ \bar{\lambda}_1^3 \bar{\lambda}_2^3 \omega_1^2 \left[\left(\mathrm{T}_{\bar{3}}^{1} - 4\right) w^4 + \left(\mathrm{T}_{4,2}^{\bar{1},0} + {}_{4}^{4}\mathrm{L}_{\bar{1}}^{0}\right) w^2 - \bar{\lambda}_1^4 \bar{\lambda}_2^4\, \mathrm{R}_{3,\bar{1}}^{4,0}\right] \omega_2 \\
&\quad - w \left[\left({}_{\bar{8}}^{4}\mathrm{L}_{\bar{7}}^{2} + \mathrm{T}_{1,\bar{3}}^{\bar{1},0}\right) w^6 - \bar{\lambda}_1^2 \bar{\lambda}_2^2 \left(\mathrm{P}_{1,\overline{11}}^{0,7} + \mathrm{Y}_{\bar{7},\bar{8}}^{1,3} + \mathrm{L}_{\bar{8}}^{4}\right) w^4 - 2\bar{\lambda}_1^6 \bar{\lambda}_2^6 \left({}_{6}^{0}\mathrm{L}_{\bar{1}}^{0} + \mathrm{T}_{6,1}^{\bar{3},0}\right) w^2 + \bar{\lambda}_1^{10} \bar{\lambda}_2^{10} \mathrm{R}_{3,\bar{1}}^{4,0}\right] \Xi_{e1} \\
&\quad + w\, \bar{\lambda}_1^2 \bar{\lambda}_2^2\, l_3 \left[\left(\mathrm{T}_{3}^{1} + 4\right) w^6 + \left({}_{\bar{4}}^{\bar{4}}\mathrm{L}_{\bar{1}}^{1} - \mathrm{T}_{4,3}^{2,0}\right) w^4 + 2\, w^2\, \bar{\lambda}_1^4\, \bar{\lambda}_2^4\, \mathrm{R}_{3,\bar{1}}^{2,\bar{1}} + \bar{\lambda}_1^{10} \bar{\lambda}_2^{10}\right] \Xi_{f1} \Big\},
\end{aligned}
$$

where

$$
\begin{aligned}
&l_1 = \bar{\lambda}_1^4 \bar{\lambda}_2^2 - 1, \quad l_2 = \bar{\lambda}_1^2 \bar{\lambda}_2^4 - 1, \quad l_{3,4} = \bar{\lambda}_1^2 \mp \bar{\lambda}_2^2, \\
&\omega_1 = \sqrt{w^2 - \bar{\lambda}_1^4 \bar{\lambda}_2^2}, \quad \omega_2 = \sqrt{w^2 - \bar{\lambda}_1^2 \bar{\lambda}_2^4}, \quad \omega_3 = \sqrt{w^2 - 1},
\end{aligned}
$$

and the symbols

$$
\begin{aligned}
&{}_{b}^{a}\mathrm{L}_{d}^{c} = a\bar{\lambda}_1^4 \bar{\lambda}_2^2 + b\bar{\lambda}_1^2 \bar{\lambda}_2^4 + c\bar{\lambda}_1^6 \bar{\lambda}_2^2 + d\bar{\lambda}_1^2 \bar{\lambda}_2^6, \quad \mathrm{P}_{b,d}^{a,c} = a\bar{\lambda}_1^8 \bar{\lambda}_2^2 + b\bar{\lambda}_1^2 \bar{\lambda}_2^8 + c\bar{\lambda}_1^6 \bar{\lambda}_2^4 + d\bar{\lambda}_1^4 \bar{\lambda}_2^6, \\
&\mathrm{R}_{b,d}^{a,c} = c\bar{\lambda}_1^4 \bar{\lambda}_2^2 + d\bar{\lambda}_1^2 \bar{\lambda}_2^4 + a\bar{\lambda}_1^2 \bar{\lambda}_2^2 + b, \qquad \mathrm{T}_{b,d}^{a,c} = a\bar{\lambda}_1^2 + b\bar{\lambda}_2^2 + c\bar{\lambda}_1^2 \bar{\lambda}_2^2 + d\bar{\lambda}_1^4 \bar{\lambda}_2^4, \\
&\mathrm{Y}_{b,d}^{a,c} = a\bar{\lambda}_1^4 + b\bar{\lambda}_2^4 + c\bar{\lambda}_1^2 \bar{\lambda}_2^2 + d\bar{\lambda}_1^4 \bar{\lambda}_2^4, \qquad \mathrm{L}_{d}^{c} = {}_{0}^{0}\mathrm{L}_{d}^{c}, \;\; {}_{b}^{a}\mathrm{L} = {}_{b}^{a}\mathrm{L}_{0}^{0}, \;\; \mathrm{T}_{b}^{a} = \mathrm{T}_{b,0}^{a,0},
\end{aligned}
$$

are introduced for brevity, with barred subscript/superscript indicating negative coefficients. Moreover, $\Xi_{f1,2}$, $\Xi_{e1,2}$, Ξ_{p3} are given in terms of the incomplete elliptic integrals of the first, second and third kind [1], respectively, via

$$
\begin{aligned}
&\Xi_{f1} = F\left(\frac{\omega_2}{w}, \omega_4\right), \quad \Xi_{f2} = F\left(\frac{\omega_1}{w}, \omega_5\right), \\
&\Xi_{e1} = E\left(\frac{\omega_2}{w}, \omega_4\right), \quad \Xi_{e2} = E\left(\frac{\omega_1}{w}, \omega_5\right), \quad \Xi_{p3} = P\left(\frac{\omega_2}{w}, \frac{\omega_3^2}{\omega_2^2}, \omega_4\right),
\end{aligned}
$$

where $\omega_{4,5} = \sqrt{\omega_{1,2}^2/\omega_{2,1}^2}$, the functions F and P are defined in (44), and the function E is defined by

$$
E(a,b) = \int_0^a \frac{\sqrt{1 - b^2 t^2}}{\sqrt{1 - t^2}}\, dt. \tag{C1}
$$

It is important to note that the components of the $\mathbf{P}_r$ tensors, given in this appendix, are valid for both prolate ($w > 1$) and oblate ($w < 1$) shapes of particles, and for all positive stretches $\bar{\lambda}_1$, and $\bar{\lambda}_2$. However, for the axisymmetric case with the condition $\bar{\lambda}_1 = \bar{\lambda}_2$ suitable limits must be taken. The final results for this case (in terms of the components of the $\mathbf{E}$ tensor) are given in Subsection 4.2. Finally, it should be pointed out that the remaining non-zero components of the tensors $\mathbf{P}_r$, such as $(P_r)_{1313}$ and $(P_r)_{1113}$, have not been provided here since they do not enter the process for calculating the appropriate components of the tensor $\mathbf{E}$, required for determining the effective stored-energy function (35).

Appendix D. On the modulus tensor $\mathbf{L}^c$ for the incompressible composites with the effective stored-energy function $\widehat{\Phi}(\bar{\lambda}_1,\bar{\lambda}_2,\bar{\theta}_2,\bar{\theta}_1)$ subjected to non-aligned loadings

In this appendix, we spell out the explicit expressions for the all traces of the effective incremental moduli tensor $\mathbf{L}^c$ which appear in the condition (47). Note that in the incompressibility limit of the composite, these (3-D) moduli traces remain finite while some components of the tensor $\widehat{\mathbf{L}}^c$ tend to infinity. Also, these traces, associated with the loading condition (24) (recall that $\bar{\theta}_1 = 0^\circ$), can be given in terms of kinematical variables $\bar{\lambda}_1, \bar{\lambda}_2, \bar{\theta}(=\bar{\theta}_2)$, as well as the derivatives of the effective potential $\widehat{\Phi}(\bar{\lambda}_1, \bar{\lambda}_2, \bar{\theta}_1, \bar{\theta}_2)$, with respect to its arguments, calculated at $\bar{\theta}_1 = 0^\circ$. Moreover, the explicit expressions for the corresponding moduli can be provided in a simpler and shorter form if they are given in a coordinate basis $\{\mathbf{e}'_i\}$ which is aligned with the loading axes (see Fig 3a). In this case, the components of the moduli tensor $\widehat{\mathbf{L}}^c$ in the basis $\{\mathbf{e}'_i\}$ and $\{\mathbf{e}_i\}$ can be related to each other thorough the following transformation rule

$$\widehat{L}'^c_{ijkl}(\bar{\mathbf{F}}) = \bar{Q}_{mi}\bar{Q}_{nj}\bar{Q}_{pk}\bar{Q}_{ql}\widehat{L}^c_{mnpq}(\bar{\mathbf{F}}), \tag{D1}$$

where $\bar{\mathbf{Q}} = \cos(\bar{\theta})\,(\mathbf{e}_1\otimes\mathbf{e}_1+\mathbf{e}_3\otimes\mathbf{e}_3)+\sin(\bar{\theta})\,(\mathbf{e}_1\otimes\mathbf{e}_3-\mathbf{e}_3\otimes\mathbf{e}_1)+\mathbf{e}_2\otimes\mathbf{e}_2$, and the primed components denote those relative to the basis $\{\mathbf{e}'_i\}$. Making use of this transformation, the aforementioned traces of $\widehat{\mathbf{L}}^c$ in the basis $\{\mathbf{e}'_i\}$ read as

$$\begin{aligned}
\widehat{L}'^*_1 &= \frac{\bar{\lambda}_1^2\,\bar{\lambda}_2\left[\left(\bar{\lambda}_1^4\bar{\lambda}_2^2+3\right)\widehat{\Phi}_{,\bar{\theta}_2}-\bar{\lambda}_1\,l_1\,\widehat{\Phi}_{,\bar{\lambda}_1\bar{\theta}_2}\right]}{l_1^2}\\
\widehat{L}'^*_2 &= \frac{\bar{\lambda}_1^2\,\bar{\lambda}_2\left[\left(3\,\bar{\lambda}_1^4\bar{\lambda}_2^2+1\right)\widehat{\Phi}_{,\bar{\theta}_2}-\bar{\lambda}_1\,l_1\,\widehat{\Phi}_{,\bar{\lambda}_1\bar{\theta}_2}\right]}{l_1^2}\\
\widehat{L}'^*_3 &= \frac{\bar{\lambda}_1\left(\bar{\lambda}_1\,l_1^2\,\widehat{\Phi}_{,\bar{\lambda}_1\bar{\lambda}_1}-2\,l_1\,\widehat{\Phi}_{,\bar{\lambda}_1}-2\,\bar{\lambda}_1^3\,\bar{\lambda}_2^2\,\widehat{\Phi}_{,\bar{\theta}_2\bar{\theta}_2}\right)}{l_1^2}\\
\widehat{L}'^c_{1313} &= \frac{\bar{\lambda}_1\left(\bar{\lambda}_1^3\,\bar{\lambda}_2^2\,\widehat{\Phi}_{,\bar{\theta}_2\bar{\theta}_2}+l_1\,\widehat{\Phi}_{,\bar{\lambda}_1}\right)}{l_1^2}\quad \widehat{L}'^c_{3131} = \frac{\bar{\lambda}_1^4\bar{\lambda}_2^2\left(\widehat{\Phi}_{,\bar{\theta}_2\bar{\theta}_2}+\bar{\lambda}_1\,l_1\,\widehat{\Phi}_{,\bar{\lambda}_1}\right)}{l_1^2}
\end{aligned} \tag{D2}$$

$$\begin{aligned}
\widehat{L}'^c_{3232} &= \frac{\bar{\lambda}_1^2\bar{\lambda}_2^4\left(\cos^2(\bar{\theta})\,\widehat{\Phi}_{,\bar{\theta}_1\bar{\theta}_1}+\bar{\lambda}_2\,l_2\,\widehat{\Phi}_{,\bar{\lambda}_2}+\sin(\bar{\theta})\cos(\bar{\theta})\,\widehat{\Phi}_{,\bar{\theta}_2}\right)}{l_2^2}\\
\widehat{L}'^c_{2323} &= \frac{\bar{\lambda}_2\left(\bar{\lambda}_1^2\,\bar{\lambda}_2^3\cos^2(\bar{\theta})\,\widehat{\Phi}_{,\bar{\theta}_1\bar{\theta}_1}+l_2\,\widehat{\Phi}_{,\bar{\lambda}_2}+\bar{\lambda}_1^2\,\bar{\lambda}_2^3\sin(\bar{\theta})\cos(\bar{\theta})\,\widehat{\Phi}_{,\bar{\theta}_2}\right)}{l_2^2}\\
\widehat{L}'^c_{2121} &= -\frac{\bar{\lambda}_1^2\left[l_3\left(\bar{\lambda}_2\,\widehat{\Phi}_{,\bar{\lambda}_2}-\bar{\lambda}_1\,\widehat{\Phi}_{,\bar{\lambda}_1}\right)+\bar{\lambda}_2^2\sin(\bar{\theta})\cos(\bar{\theta})\,\widehat{\Phi}_{,\bar{\theta}_2}-\bar{\lambda}_2^2\sin^2(\bar{\theta})\,\widehat{\Phi}_{,\bar{\theta}_1\bar{\theta}_1}\right]}{l_3^2}\\
\widehat{L}'^c_{1212} &= -\frac{\bar{\lambda}_2^2\left[l_3\left(\bar{\lambda}_2\,\widehat{\Phi}_{,\bar{\lambda}_2}-\bar{\lambda}_1\,\widehat{\Phi}_{,\bar{\lambda}_1}\right)+\bar{\lambda}_1^2\sin(\bar{\theta})\cos(\bar{\theta})\,\widehat{\Phi}_{,\bar{\theta}_2}-\bar{\lambda}_1^2\sin^2(\bar{\theta})\,\widehat{\Phi}_{,\bar{\theta}_1\bar{\theta}_1}\right]}{l_3^2}
\end{aligned} \tag{D3}$$

$$\widehat{L}_4^{\prime *} = \frac{\left(\bar{\lambda}_2\, l_2^2\, \widehat{\Phi}_{,\lambda_2\lambda_2} - 2\, l_2\, \widehat{\Phi}_{,\bar{\lambda}_2} - 2\,\bar{\lambda}_1^2\,\bar{\lambda}_2^3\,\sin\left(\bar{\theta}\right)\cos(\bar{\theta})\,\widehat{\Phi}_{,\bar{\theta}_2} - 2\,\bar{\lambda}_1^2\bar{\lambda}_2^3\,\cos^2(\bar{\theta})\,\widehat{\Phi}_{,\bar{\theta}_1\bar{\theta}_1}\right)\bar{\lambda}_2}{l_2^2}$$

$$\begin{aligned}\widehat{L}_5^{\prime *} = -(l_1^2 l_2^2 l_3^2)^{-1}\Big\{&\bar{\lambda}_1^2\bar{\lambda}_2^2\left(\bar{\lambda}_1^4\bar{\lambda}_2^8 + \bar{\lambda}_1^4\bar{\lambda}_2^2 - 4\,\bar{\lambda}_1^2\bar{\lambda}_2^4 + \bar{\lambda}_2^6 + 1\right) l_1^2\,\sin(\bar{\theta})\cos(\bar{\theta})\,\widehat{\Phi}_{,\bar{\theta}_2}\\ &+ \bar{\lambda}_1^2\bar{\lambda}_2^2 l_1^2\left[\left(\bar{\lambda}_1^4\bar{\lambda}_2^8 + \bar{\lambda}_1^4\bar{\lambda}_2^2 - 4\,\bar{\lambda}_1^2\bar{\lambda}_2^4 + \bar{\lambda}_2^6 + 1\right)\cos^2(\bar{\theta}) - l_2^2\right]\widehat{\Phi}_{,\bar{\theta}_1\bar{\theta}_1}\\ &- \bar{\lambda}_1\,\bar{\lambda}_2\, l_1^2 l_2^2 l_3^2\,\widehat{\Phi}_{,\bar{\lambda}_1\bar{\lambda}_2} + \bar{\lambda}_1^4\bar{\lambda}_2^2 l_2^2 l_3^2\,\widehat{\Phi}_{,\bar{\theta}\,\bar{\theta}} - \bar{\lambda}_1^3\, l_1\, l_2^3\, l_3\,\widehat{\Phi}_{,\bar{\lambda}_1} + \bar{\lambda}_2^3\, l_1^3\, l_2^2\, l_3\,\widehat{\Phi}_{,\bar{\lambda}_2}\Big\}\end{aligned} \tag{D4}$$

$$\begin{aligned}\widehat{L}^{\prime c}_{2312} = \widehat{L}^{\prime c}_{3212} = \widehat{L}^{\prime c}_{3221} &= -\frac{\left[\left(l_1\cos^2(\bar{\theta}) - \bar{\lambda}_1^2\bar{\lambda}_2^2 l_3\right)\widehat{\Phi}_{,\bar{\theta}_2} - \sin(\bar{\theta})\cos(\bar{\theta}) l_1\,\widehat{\Phi}_{,\bar{\theta}_1\bar{\theta}_1}\right]\bar{\lambda}_1^2\bar{\lambda}_2^3}{l_1^2\, l_2^2\, l_3}\\ \widehat{L}^{\prime c}_{2321} &= -\frac{\left[\left(\bar{\lambda}_2^2 l_1\cos^2(\bar{\theta}) - \bar{\lambda}_1^2 + \bar{\lambda}_2^2\right)\widehat{\Phi}_{,\bar{\theta}_2} - \sin(\bar{\theta})\cos(\bar{\theta})\bar{\lambda}_2^2 l_1\,\widehat{\Phi}_{,\bar{\theta}_1\bar{\theta}_1}\right]\bar{\lambda}_1^2\bar{\lambda}_2}{l_3\, l_2^2 l_1^2}\end{aligned} \tag{D5}$$

$$\begin{aligned}\widehat{L}_6^{\prime *} &= -(l_1^2\, l_2\, l_3)^{-1}\,\bar{\lambda}_1^2\bar{\lambda}_2\\ &\times\left\{\left[\bar{\lambda}_2^2 l_1^2\cos^2(\bar{\theta}) - l_3\left(2\,\bar{\lambda}_1^6\bar{\lambda}_2^6 - l_1\right)\right]\widehat{\Phi}_{,\bar{\theta}_2} + \bar{\lambda}_2\, l_1\, l_2\, l_3\,\widehat{\Phi}_{,\lambda_2\theta} - \bar{\lambda}_2^2 l_1^2\,\sin(\bar{\theta})\cos(\bar{\theta})\,\widehat{\Phi}_{,\bar{\theta}_1\bar{\theta}_1}\right\}\\ \widehat{L}_7^{\prime *} &= -(l_3\, l_2\, l_1^2)^{-1}\,\bar{\lambda}_1^2\bar{\lambda}_2\\ &\times\left\{\left[\bar{\lambda}_2^2 l_1^2\cos^2(\bar{\theta}) - l_3\left(\bar{\lambda}_1^6\bar{\lambda}_2^6 + \bar{\lambda}_1^2\bar{\lambda}_2^4 - 2\right)\right]\widehat{\Phi}_{,\bar{\theta}_2} + \bar{\lambda}_2\, l_1\, l_2\, l_3\,\widehat{\Phi}_{,\bar{\lambda}_2\bar{\theta}} - \bar{\lambda}_2^2 l_1^2\,\sin(\bar{\theta})\cos(\bar{\theta})\,\widehat{\Phi}_{,\bar{\theta}_1\bar{\theta}_1}\right\}\\ \widehat{L}_8^{\prime *} &= -(l_3\, l_2\, l_1^2)^{-1}\,\bar{\lambda}_1^2\bar{\lambda}_2\\ &\times\Big\{\left[\bar{\lambda}_2^2 {l_1}^2\cos^2(\bar{\theta}) - l_3\left(5\,\bar{\lambda}_1^6\bar{\lambda}_2^6 - 4\,\bar{\lambda}_1^4\bar{\lambda}_2^2 + \bar{\lambda}_1^2\bar{\lambda}_2^4 - 2\right)\right]\widehat{\Phi}_{,\bar{\theta}_2} + l_1\, l_2\, l_3\left(\bar{\lambda}_1\,\widehat{\Phi}_{,\lambda_1\bar{\theta}} + \bar{\lambda}_2\,\widehat{\Phi}_{,\bar{\lambda}_2\bar{\theta}}\right)\\ &-\bar{\lambda}_2^2 l_1^2\,\sin(\bar{\theta})\cos(\bar{\theta})\,\widehat{\Phi}_{,\bar{\theta}_1\bar{\theta}_1}\Big\}\end{aligned} \tag{D6}$$

Note that for axisymmetric shear loadings with the condition $\bar{\lambda}_1 = \bar{\lambda}_2 = \bar{\lambda}$, suitable limits must be taken for the traces involving the terms $(\bar{\lambda}_1 - \bar{\lambda}_2)$ in the denominator. Taking these limits for the pertinent traces appearing in the strong ellipticity condition (56) yields

$$\begin{aligned}\widehat{L}^{\prime c}_{2121} &= \frac{1}{8}\,\bar{\lambda}\,\Big[\bar{\lambda}\,\sin^2(\bar{\theta})\widehat{\Phi}_{,\bar{\lambda}_1\bar{\lambda}_1\bar{\theta}_1\bar{\theta}_1} + 6\,\bar{\lambda}\,\widehat{\Phi}_{,\bar{\lambda}_1\bar{\lambda}_1} + 2\,\bar{\lambda}\,\widehat{\Phi}_{,\bar{\lambda}_2\bar{\lambda}_2} - 2\,\bar{\lambda}\,\widehat{\Phi}^{AS}_{,\bar{\lambda}\bar{\lambda}} + 8\,\widehat{\Phi}_{,\bar{\lambda}_1}\\ &\quad -2\,\widehat{\Phi}^{AS}_{,\bar{\lambda}} - \bar{\lambda}\,\sin(\bar{\theta})\cos(\bar{\theta})\widehat{\Phi}_{,\bar{\lambda}_1\bar{\lambda}_1\bar{\theta}}\Big]\Big|_{\bar{\lambda}_1=\bar{\lambda}_2=\bar{\lambda}}\\ \widehat{L}^{\prime c}_{2321} &= -\frac{1}{2}\,\bar{\lambda}^2\left(\bar{\lambda}^6 - 1\right)^{-2}\Big\{2\,\bar{\lambda}\left(2\,\bar{\lambda}^6\cos^2(\bar{\theta}) - 1\right)\widehat{\Phi}_{,\bar{\theta}} + \bar{\lambda}^2\left(\bar{\lambda}^6 - 1\right)\cos^2(\bar{\theta})\widehat{\Phi}_{,\bar{\lambda}_1\bar{\theta}}\\ &\quad -\bar{\lambda}^2\,\sin(\bar{\theta})\cos(\bar{\theta})\left[\left(\bar{\lambda}^6 - 1\right)\widehat{\Phi}_{,\bar{\lambda}_1\bar{\theta}_1\bar{\theta}_1} + 4\,\bar{\lambda}^5\,\widehat{\Phi}_{,\bar{\theta}_1\bar{\theta}_1}\right]\Big\}\Big|_{\bar{\lambda}_1=\bar{\lambda}_2=\bar{\lambda}}\end{aligned}$$

For the special case of aligned loadings ($\bar{\theta} = 0^\circ$), the above expressions for the moduli traces simplify considerably. For convenience in using these traces in the SE condition (50) (associated with aligned loadings), we provide the simplified expressions. The relevant, non-zero traces in the basis $\{\mathbf{e}_i\}$ (note that $\widehat{L}^{\prime c}_{ijkl} = \widehat{L}^{c}_{ijkl}$ for aligned loadings) read

as

$$\widehat{L}_3^* = \frac{\bar{\lambda}_1 \left(\bar{\lambda}_1 l_1^2 \widehat{\Phi}_{,\bar{\lambda}_1\bar{\lambda}_1} - 2 l_1 \widehat{\Phi}_{,\bar{\lambda}_1} - 2\bar{\lambda}_1^3 \bar{\lambda}_2^2 \widehat{\Phi}_{,\bar{\theta}_2\bar{\theta}_2} \right)}{l_1^2},$$

$$\widehat{L}^c_{1313} = \frac{\bar{\lambda}_1 \left(\bar{\lambda}_1^3 \bar{\lambda}_2^2 \widehat{\Phi}_{,\bar{\theta}_2\bar{\theta}_2} + l_1 \widehat{\Phi}_{,\bar{\lambda}_1} \right)}{l_1^2}, \quad \widehat{L}^c_{3131} = \frac{\bar{\lambda}_1^4 \bar{\lambda}_2^2 \left(\widehat{\Phi}_{,\bar{\theta}_2\bar{\theta}_2} + \bar{\lambda}_1 l_1 \widehat{\Phi}_{,\bar{\lambda}_1} \right)}{l_1^2}, \tag{D7}$$

$$\widehat{L}^c_{3232} = \frac{\bar{\lambda}_1^2 \bar{\lambda}_2^4 \left(\widehat{\Phi}_{,\bar{\theta}_1\bar{\theta}_1} + \bar{\lambda}_2 l_2 \widehat{\Phi}_{,\bar{\lambda}_2} \right)}{l_2^2}, \quad \widehat{L}^c_{2323} = \frac{\bar{\lambda}_2 \left(\bar{\lambda}_1^2 \bar{\lambda}_2^3 \widehat{\Phi}_{,\bar{\theta}_1\bar{\theta}_1} + l_2 \widehat{\Phi}_{,\bar{\lambda}_2} \right)}{l_2^2},$$

$$\widehat{L}^c_{2121} = \frac{\bar{\lambda}_1^2 \left(\bar{\lambda}_1 \widehat{\Phi}_{,\bar{\lambda}_1} - \bar{\lambda}_2 \widehat{\Phi}_{,\bar{\lambda}_2} \right)}{l_3^2}, \quad \widehat{L}^c_{1212} = \frac{\bar{\lambda}_2^2 \left(\bar{\lambda}_1 \widehat{\Phi}_{,\bar{\lambda}_1} - \bar{\lambda}_2 \widehat{\Phi}_{,\bar{\lambda}_2} \right)}{l_3}, \tag{D8}$$

$$\widehat{L}_4^* = \frac{\bar{\lambda}_2 \left(\bar{\lambda}_2 l_2^2 \widehat{\Phi}_{,\bar{\lambda}_2\bar{\lambda}_2} - 2 l_2 \widehat{\Phi}_{,\bar{\lambda}_2} - 2\bar{\lambda}_1^2 \bar{\lambda}_2^3 \widehat{\Phi}_{,\bar{\theta}_1\bar{\theta}_1} \right)}{l_2^2},$$

$$\widehat{L}_5^* = (l_1^2 l_2^2 l_3)^{-1} \left[\bar{\lambda}_1 \bar{\lambda}_2 l_1^2 l_2^2 l_3 \widehat{\Phi}_{,\bar{\lambda}_1\bar{\lambda}_2} - \bar{\lambda}_1^2 \bar{\lambda}_4^2 l_1^2 l_3 \widehat{\Phi}_{,\bar{\theta}_1\bar{\theta}_1} - \bar{\lambda}_1^4 \bar{\lambda}_2^2 l_2^2 l_3 \widehat{\Phi}_{,\bar{\theta}_2\bar{\theta}_2} + \bar{\lambda}_1^3 l_1 l_2^3 \widehat{\Phi}_{,\bar{\lambda}_1} - \bar{\lambda}_2^3 l_2 l_1^3 \widehat{\Phi}_{,\bar{\lambda}_2} \right]. \tag{D9}$$

Again, note that for axisymmetric shear loadings with the condition $\bar{\lambda}_1 = \bar{\lambda}_2 = \bar{\lambda}$, suitable limits must be taken for the traces involving the terms $(\bar{\lambda}_1 - \bar{\lambda}_2)$ in the denominator. Taking these limits for the pertinent traces appearing in the SE condition (50) yields

$$\widehat{L}^c_{1212} = \widehat{L}^c_{2121} = \frac{1}{2}\bar{\lambda} \left[\frac{1}{2} \widehat{\Phi}^{AS}_{,\bar{\lambda}} + \bar{\lambda} \left(2\widehat{\Phi}_{,\bar{\lambda}_1\bar{\lambda}_1} - \frac{1}{2} \widehat{\Phi}^{AS}_{,\bar{\lambda}\bar{\lambda}} \right) \Big|_{\bar{\lambda}_1 = \bar{\lambda}_2 = \bar{\lambda}} \right],$$

$$\widehat{L}_5^* = \frac{1}{4} \frac{\bar{\lambda} \left[\left(\bar{\lambda}^{13} - 2\bar{\lambda}^7 + \bar{\lambda} \right) \widehat{\Phi}^{AS}_{,\bar{\lambda}\bar{\lambda}} - 4\bar{\lambda}^5 \left(\widehat{\Phi}_{,\bar{\theta}_1\bar{\theta}_1} + \widehat{\Phi}_{,\bar{\theta}\bar{\theta}} \right) - \left(\bar{\lambda}^{12} + 2\bar{\lambda}^6 - 3 \right) \widehat{\Phi}^{AS}_{,\bar{\lambda}} \right]}{\left(\bar{\lambda}^6 - 1 \right)^2}.$$

References

[1] Abramowitz, M., Stegun, I., 1965. Handbook of Mathematical functions with formulas, graphs, and mathematical tables. Dover, New York.

[2] Agoras, M., Lopez-Pamies, O., Ponte Castañeda, P., 2009a. A general hyperelastic model for incompressible fiber-reinforced elastomers. J. Mech. Phys. Solids 57, 268–286.

[3] Agoras, M., Lopez-Pamies, O., Ponte Castañeda, P., 2009b. Onset of macroscopic instabilities in fiber-reinforced elastomers at finite strain. J. Mech. Phys. Solids 57, 1828–1850.

[4] Avazmohammadi, R., Ponte Castañeda, P., 2013. Tangent second-order estimates for the large-strain, macroscopic response of particle-reinforced elastomers. J. Elasticity 112, 139–183.

[5] Avrachenkov, K., Haviv, M., Howlett, P., 2001. Inversion of analytic matrix functions that are singular at the origin. SIAM J. on Matrix Analysis and Applications 22, 1175–1189.

[6] Bergstrom, J., Boyce, M., 1999. Mechanical behavior of particle-filled elastomers. Rubber Chem. Technol. 72, 633–656.

[7] Bouchart , V., Brieu , M., Kondo, D., Nait Abdelaziz, M. 2008. Implementation and numerical verification of a non-linear homogenization method applied to hyperelastic composites. Computational Material Science 43, 670–680.

[8] Brun, M., Lopez-Pamies, O., Ponte Castañeda, P., 2007. Homogenization estimates for fiber-reinforced elastomers with periodic microstructures. Int. J. Solids Struct. 44, 5953–5979.

[9] Chen, H., Liu, Y., Zhao, X., Lanir, Y., Kassab, G., 2011. A micromechanics finite-strain constitutive model of fibrous tissue. J. Mech. Phys. Solids 59, 1823–1837.

[10] deBotton, G., 2005. Transversely isotropic sequentially laminated composites in finite elasticity. J. Mech. Phys. Solids 53, 1334–1361.

[11] deBotton, G., Hariton, I., Socolsky, E., 2006. Neo-Hookean fiber-reinforced composites in finite elasticity. J. Mech. Phys. Solids 54, 533–559.
[12] deBotton, G., Shmuel, G., 2010. A new variational estimate for the effective response of hyperelastic composites. J. Mech. Phys. Solids 58, 466–483.
[13] Gent, A., 1996. A new constitutive relation for rubber. Rubber Chem. Tech. 69, 59–61.
[14] Geymonat, G., Müller, S., Triantafyllidis, N., 1993. Homogenization of nonlinearly elastic materials, microscopic bifurcation and macroscopic loss of rank-one convexity. Arch. Rat. Mech. Anal. 122, 231–290.
[15] Hill, R., 1972. On constitutive macro-variables for heterogeneous solids at finite strain. Proc. Roy. Soc. Lon. A 326, 131–147.
[16] Lahellec, N., Mazerolle, F., Michel, J.-C., 2004. Second-order estimate of the macroscopic behavior of periodic hyperelastic composites: theory, experimental validation. J. Mech. Phys. Solids 52, 27–49.
[17] Leblanc, L., 2010. Filled Polymers: Science and Industrial Applications. CRC Press, New York.
[18] Limbert, G., Middleton, J., 2006. A constitutive model of the posterior cruciate ligament. Medical Eng. Phys. 28, 99–113.
[19] Loocke, M., Lyons, C., Simms, C., 2006. A validated model of passive muscle in compression. J. Biomech. 39, 2999–3009.
[20] Lopez-Pamies, O., Goudarzi, T., Danas, K., 2013b. The nonlinear elastic response of suspensions of rigid inclusions in rubber: II, A simple explicit approximation for finite-concentration suspensions. J. Mech. Phys. Solids 61, 19–37.
[21] Lopez-Pamies, O., Goudarzi, T., Nakamura, T., 2013a. The nonlinear elastic response of suspensions of rigid inclusions in rubber: I, An exact result for dilute suspensions. J. Mech. Phys. Solids 61, 1–18.
[22] Lopez-Pamies, O., Idiart, M., 2010. Fiber-reinforced hyperelastic solids: a realizable homogenization constitutive theory. J. Engng. Math. 68, 57–83.
[23] Lopez-Pamies, O., Ponte Castañeda, P., 2004. Second-order estimates for the macroscopic response and loss of ellipticity in porous rubbers at large deformations. J. Elasticity 76, 247–287.
[24] Lopez-Pamies, O., Ponte Castañeda, P., 2006a. On the overall behavior, microstructure evolution, and macroscopic stability in reinforced rubbers at large deformations: I - Theory. J. Mech. Phys. Solids 54, 807–830.
[25] Lopez-Pamies, O., Ponte Castañeda, P., 2006b. On the overall behavior, microstructure evolution, and macroscopic stability in reinforced rubbers at large deformations: II - Application. J. Mech. Phys. Solids 54, 831–863.
[26] Lopez-Pamies, O., Ponte Castañeda, P., 2009. Microstructure evolution in hyperelastic laminates and implications for overall behavior and macroscopic stability. Mech. Mater. 41, 364–374.
[27] Michel, J., Lopez-Pamies, O., Ponte Castañeda, P., Triantafyllidis, N., 2010. Microscopic and macroscopic instabilities in finitely strained fiber-reinforced elastomers. J. Mech. Phys. Solids 58, 1776–1803.
[28] Milton, G., 2002. The Theory of Composites. Cambridge University Press, Cambridge, U.K.
[29] Moraleda, J., Segurado, J., Llorca, J., 2009. Finite deformation of incompressible fiber-reinforced elastomers: A computational micromechanics approach. J. Mech. Phys. Solids 57, 1596–1613.
[30] O'Connor, J.E. 1977. Short-fiber-reinforced elastomer composites. Rubber Chem. Technol. 50, 945–958.
[31] Ogden, R., Saccomandi, G., Sgura, I., 2004. Fitting hyperelastic models to experimental data. Computational Mechanics 34, 484–502.
[32] Ponte Castañeda, P., 2002. Second-order homogenization estimates for nonlinear composites incorporating field fluctuations. I. Theory. J. Mech. Phys. Solids 50, 737–757.
[33] Ponte Castañeda, P., Galipeau, E., 2011. Homogenization-based constitutive models for magnetorheological elastomers at finite strain. J. Mech. Phys. Solids 59 (19), 194–215.
[34] Ponte Castañeda, P., Siboni, M. H., 2012. A finite-strain constitutive theory for electro-active polymer composites via homogenization. Int. J. of Nonlinear Mech. 47 (2), 293–306.
[35] Ponte Castañeda, P., Tiberio, E., 2000. A second-order homogenization method in finite elasticity and applications to black-filled elastomers. J. Mech. Phys. Solids 48, 1389–1411.
[36] Ponte Castañeda, P., Willis, J., 1995. The effect of spatial distribution on the effective behavior of composite materials and cracked media. J. Mech. Phys. Solids 43, 1919–1951.
[37] Quapp, K., Weiss, J., 1998. Material characterization of human medial collateral ligament. J. Biomech. Eng. 120, 757–763.
[38] Racherla, V., Lopez-Pamies, O., Ponte Castañeda, P., 2010. Macroscopic response and stability in lamellar nanostructured elastomers with "oriented" and "unoriented" polydomain microstructures. Mech. Mater. 42, 451–468.
[39] Rudykh, S., deBotton, G., 2012. Instabilities of Hyperelastic Fiber Composites: Micromechanical Versus Numerical Analyses. J. Elasticity 106, 123–147.
[40] Triantafyllidis, N., Marker, B., 1985. On the comparison between microscopic and macroscopic in stability mechanisms in a class of fiber-reinforced composites. J. Appl. Mech. 52, 794–800.
[41] Triantafyllidis, N., Nestorovic, M., Schaard, M., 2006. Failure surfaces for finitely strained two-phase periodic solids under general in-plane loading. J. Appl. Mech. 73, 505–516.
[42] Wang, M., Zhang, P., K., M., 2001. Carbon Silica dual phase filler, a new generation reinforcing agent for rubber: Part IX. application to truck tire tread compound. Rubber Chem. Tech. 74, 124–137.
[43] Willis, J., 1977. Bounds and self-consistent estimates for the overall moduli of anisotropic composites. J. Mech. Phys. Solids 25, 185–202.